# Total Ionizing Dose and Dose Rate Effects on (Positive and Negative) BJT Based Bandgap References

by

Parker Davis

A Thesis Presented in Partial Fulfillment
of the Requirements for the Degree
Master of Science

Approved April 2019 by the
Graduate Supervisory Committee:

Hugh Barnaby, Chair
Jennifer Kitchen
Aymeric Privat

ARIZONA STATE UNIVERSITY
May 2019

# ABSTRACT

Space exploration is a large field that requires high performing circuitry due to the harsh environment. Within a space environment one of the biggest factors leading to circuit failure is radiation. Circuits must be robust enough to continue operation after being exposed to the high doses of radiation. Bandgap reference (BGR) circuits are designed to be voltage references that stay stable across a wide range of supply voltages and temperatures. A bandgap reference is a piece of a large circuit that supplies critical elements of the large circuit with a constant voltage. When used in a space environment with large amounts of radiation a BGR needs to maintain its output voltage to enable the rest of the circuit to operate under proper conditions. Since a BGR is not a standalone circuit it is difficult and expensive to test if a BGR is maintaining its reference voltage.

This thesis describes a methodology of isolating and simulating bandgap references. Both NPN and PNP bandgap references are simulated over a variety of radiation doses and dose rates. This methodology will allow the degradation due to radiation of a BGR to be modeled easily and affordably. It can be observed that many circuits experience enhanced low dose rate sensitivity (ELDRS) which can lead to failure at low total ionizing doses (TID) of radiation. A compact model library demonstrating degradation of transistors at both high and low dose rates (HDR and LDR) will be used to show bandgap references reliability. Specifically, two bandgap references being utilized in commercial off the shelf low dropout regulators (LDO) will be evaluated. The LDOs are reverse engineered in a simulation program with integrated circuit emphasis (SPICE). Within the two LDOs the bandgaps will be the points of interest. Of the LDOs one has a

positive regulated voltage and one has a negative regulated voltage. This requires an NPN and a PNP based BGR respectively. This simulation methodology will draw conclusions about the above bandgap references, and how they operate under radiation at different doses and dose rates.

# ACKNOWLEDGMENTS

I would like to thank my advisor, Dr. Hugh Barnaby, for his guidance and technical discussions provided throughout the completion of work described in this thesis. His thought-provoking questions and attention to detail challenged me to achieve more. He always considers the interests of his students to make sure everyone gets a project they that they will enjoy. I would also like to thank Aymeric Privat for his technical contributions which helped make the work presented in this thesis possible. He was always available to answer my questions and explain any points of confusion.

I would like to thank my family, Mom, Dad and Alexis, for their support. You have pushed me to be the driven person I am today. Finally, I would like to thank Larissa for always listening to my struggles and helping me stay calm throughout this process. You always helped me see the finish line no matter how far away it was. Additionally, I would like to thank my close friends who have always been there for me.

Thank you all.

TABLE OF CONTENTS

Page

LIST OF TABLES

Table Page

LIST OF FIGURES

Figure Page

# CHAPTER 1 INTRODUCTION TO BANDGAP REFERENCES

## *1.1 Historical Perspective*

For many analog and mixed signal (A/MS) integrated circuits (IC) producing accurate signals with low noise and distortion is critical. However, for A/MS circuits operating in extreme environments, maintaining a high level of precision over wide temperature ranges and high levels of radiation can be difficult. One example of an extreme environment is space. Space can expose circuits to very large temperature fluctuations as well as to large doses of radiation over time. One critical piece of circuitry for provided temperature stability in A/MS circuits is the bandgap reference (BGR). The BGR is designed to provide a stable reference voltage for many components in an IC [1-4]. Bandgap references are designed to be both supply and (mostly) temperature independent within a specified range. Therefore, if there is a temperature shift in the environment the BGR will hold its voltage and allow the rest of the circuit to operate properly.

Radiation exposure in space has shown to cause many types of A/MS ICs to fail, including linear bipolar circuits that use BGRs composed solely of bipolar junction transistors (BJTs) [2], [6-20], [23], [44], [48], [54]. Exposure to a total ionizing dose (TID) of radiation degrades the current gain of BJTs which can cause the BJT-based bandgap reference voltage to drift out of specification. BJTs and linear bipolar circuits are also susceptible to enhanced low dose rate sensitivity (ELDRS). This means that BJTs will degrade more rapidly as a function of TID when exposed to a low dose rate (LDR) compared to a high dose rate (HDR) [7-9], [14], [17-19], [21-23], [26], [29], [37], [40-43].

One of the most basic temperature independent voltage references developed was a Zener diode reference. Although this design works, it requires a supply voltage large enough to breakdown the Zener diode. Therefore, for most technologies it is only practical for supply voltages greater than 7V [1]. Once the Zener diode is put into an avalanche breakdown mode its resistance is negligible and it act as a near zero temperature coefficient (TC) voltage source [1-5]. Still, for the Zener diode reference a temperature independent voltage source is required. This is where a supply independent BGR becomes necessary.

Bandgap references were first introduced in 1971 by Robert Widlar, but were they quickly improved upon by Paul Brokaw [2]. The Brokaw cell enables the BGR to perform at both high and low supply voltages. The Brokaw cell's high voltage capabilities removes the need for any Zener references. The cell set the stage for the future of almost all BGRs. To be used in most linear analog circuits, bandgap references need to operate at low and high supply voltages without losing their temperature insensitivity. The basic idea behind a bandgap reference is to cancel the negative TC of a BJT's base emitter voltage with the positive TC of the thermal voltage. This process in theory will allow for a total TC near zero. Fig. 1 provides a conceptual illustration for how a BGR is implemented.

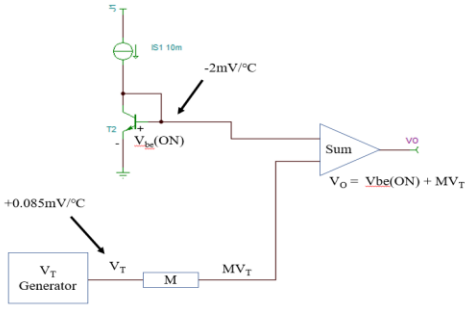


*Fig. 1 Hypothetical BGR [1]*

This conceptual BGR schematic shows how the temperature dependences of the BJT's $V_{be(ON)}$ and thermal voltage, $V_T$, can effectively offset each other. The thermal voltage, $V_T$, is equal to kT/q = 0.2586 V at 300K, where k is Boltzmann's constant, q is the magnitude of electronic charge, and T is the lattice temperature. At 300K $V_O$ is typically 1.21V (near the bandgap energy of silicon) which is the sum of the ≈0.6V from the $V_{be(ON)}$ summed with an amplified version of thermal voltage. The amplification will bring the TC of $V_T$ to nearly 2mV/ ℃ to create the overall TC of 0 V/ ℃.

The Brokaw cell does come with a few minor downsides one being TC curvature and the other being noise. These bandgaps exhibit a positive TC at high temperatures and a negative TC at low temperatures [2]. This TC change can shift the reference voltage by about +/- 1% depending on the temperature. Secondly, the summing amplifier requies a large gain which drastically increases noise generated from the BJT's. This limits a BGR's practicality within noise sensitive circuits like high resolution analog to digital converters (ADC) [2]. With careful design many drawbacks of the BGR can be mitigated at the cost of making a more complex circuit.

*1.2 Bandgap Reference Design Considerations*

A bandgap reference uses a combination of proportional to absolute temperature (PTAT) and complementary to absolute temperature (CTAT) references. PTAT references increase with temperature and CTAT references decrease with temperature. A BGR will use the sum of the CTAT and PTAT currents to reach close to temperature independence within a certain temperature range [4]. BGRs utilize a combination of two transistors with

different emitter current densities. One BJT will typically run at an 8-10 times larger current density than the other. This creates a

voltage differential (≈60mV at 300K, or 27°C) which is then amplified and added to a $V_{BE}$ to get the reference voltage of the BGR [2]. A full analysis of one type Brokaw cell design is provided below.

As mentioned above an ideal BGR should have a low TCF with both long- and short-term stability. A BGR also needs to be insensitive to loading since in almost all cases a BGR will be supplying other blocks within a large circuit [3].

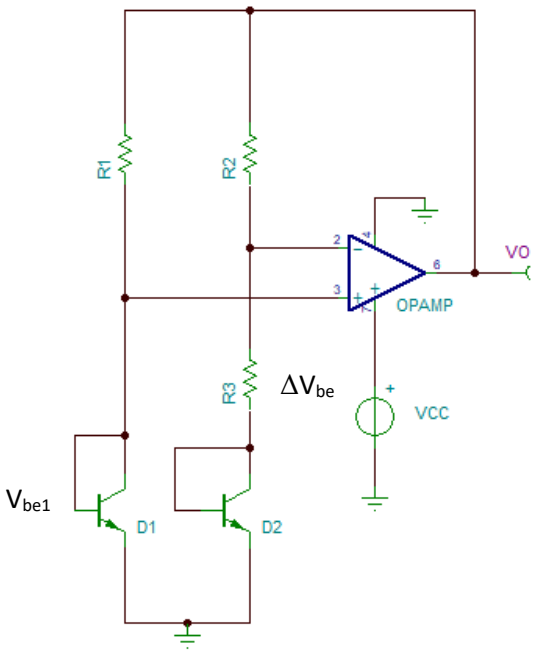


*Fig. 2 Brokaw Cell [3]*

Fig. 2 illustrates a simple Brokaw cell design. It contains two diode connected BJT's and an amplifier. In the Brokaw cell the output reference, $V_O$, is set by $V_{be1}$ and a resistor ratio.

Due to the opamps virtual short we can expect $V_{be1}$ on both the positive and negative terminals. This introduces a $\Delta V_{be}$ across resistor $R_3$. $V_O$ can be modeled as a sum of $V_{be1}$ and a gain of $M*\Delta V_{be}$, where M is set by the resistor ratio $(R_2 + R_3)/R_3$. A more general function for $V_O$ specific to the BGR circuit is given in Eq. 2 below where the $V_{GO}$ term is the approximate bandgap voltage of

$$V_0 = V_{GO} + (\eta - 1)\frac{kT}{q} - (\eta - 1)\frac{kT}{q}\ln(\frac{T}{T_0}) \quad (1)$$

silicon at 0K (1.21V). This equation reveals the positive and negative temperature dependent factors of the BGR output. In Eq. 2 $\eta = 4-n$ where n is a parameter dependent on the doping concentration and $T_0$, which is the temperature at $dV_O/dT = 0V/ ℃$ [3]. Typically, $T_0$ is set between 25 ℃ and 28 ℃. The functional dependence of $V_O$ and T is roughly parabolic near $T_0$. It can be seen in Eq. 2 that when $T = T_0$ then $V_O = V_{GO} + \alpha V_T$. At $T = T_0$ there is ideally total temperature independence. This parabolic relationship between $V_O$ and T is illustrated in Fig. 3.

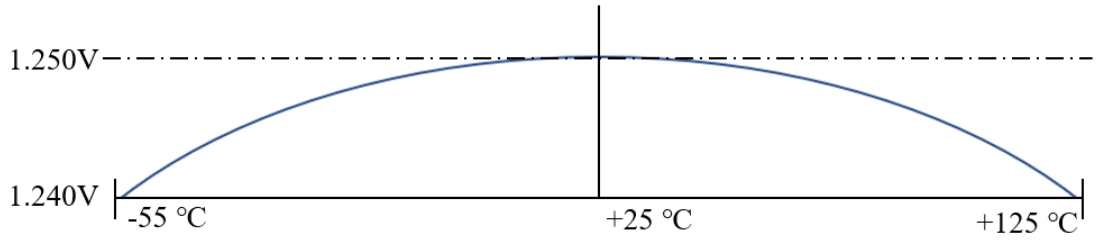


*Fig. 3 Parabolic Temperature Relationship [2]*

The small concavity of the function near $T_0$ is acceptable since if the temperature ranges from -55℃ to 125 ℃ there are only small changes in $V_O$ (<10mV). An additional source of error comes from the opamp's voltage drift [3]. Voltage drift of the amplifier

shifts the entire parabolic curve of the BGR. To compensate for this more diode pairs can be added along with a preamplifier stage [3]. Designing a low drift amplifier will greatly increase the temperature stability of the BGR.

A BGR often acts as a startup for many of the blocks on a single integrated circuit [2]. Therefore, a BGR needs to start up promptly so that it may power the rest of the system [2]. This calls for a highly reliable startup circuit to get the BGR running. Startup circuits are designed to provide initial biasing for many of the transistors within the BGR. After the startup toggles the BGR to its targeted reference voltage, it should draw little to no power.

*1.3 Overview of Bandgap Reference Reliability Concerns Related to NPN vs PNP*

A typical BGR is composed of an amplifier and a transistor pair. Each block needs to be working properly to achieve optimal performance. The amplifier is used to provide feedforward gain to the small voltage difference generated by the different current densities through the transistor pair. This amplifier's gain will be a main factor in setting the reference voltage. This can be used as a benefit to select a specify desired reference voltage. If the opamp is not working properly the BGR will set an incorrect reference voltage and will likely exhibit greater temperature sensitivity.

Within a BGR there are critical transistors that must be carefully placed to ensure operational stability [8]. Due to the bandgap reference's importance to the A/MS circuit, it is crucial to select a BGR that is the most resistant to all forms of degradation. In this thesis, two BGR architectures will be investigated based on NPN and a PNP topology. The PNP-

based BGR is used in a negative voltage low dropout regulator (LDO), e.g. the LT1175, which requires a negative reference voltage. The LT1175 has a supply range down to -20V. It needs a BGR supplied reference voltage of -3.8V across this supply range. The NPN critical transistor BGR is used in a positive regulating LDO, e.g. the LP2953. This LDO has a supply of 2.3-30V and the NPN BGR must maintain its 1.22V reference across the supply range.

*1.4 Goals and Approach*

This thesis will discuss the robustness of both BGR types to TID. Test and modeling results on two commercial-off-the-shelf (COTS) linear bipolar parts, the LT1175 and LP2953, that use one or the other BGR types will be presented. Both parts are low dropout regulators (LDO) and require BGRs to perform their functions. The LT1175 regulates a negative voltage utilizing a PNP pair for the BGR, and the LP2953 regulates a positive voltage with an NPN pair in the BGR. Analysis of the standalone BGR and its implementation in the LDOs will show if any significant differences exist between the two types of BGRs after they have been irradiated. The data and analysis gathered will provide information as to which BGR may be more reliable in high radiation environments. This may allow engineers to quickly chose a circuit for a project based on its bandgap reference type. The circuits and models developed will also grant a cheaper method for verifying an irradiated circuits long term reliability in extreme environments.

This project will use a large database of post-irradiation NPN and PNP characteristics that were obtained from experiments or models. With this database, compact models are developed to simulate degraded BJTs in circuits as a function of TID at both

HDR and LDR. Circuit modeling with SPICE can help mitigate the costs of irradiating and testing actual hardware.

# CHAPTER 2 RADIATION EFFECTS BACKGROUND

## *2.1 Total Ionizing Dose Effects: Radiation-induced Defects*

Radiation in the space environment can cause transient errors and permanent changes to semiconductors material parameters. In space the primary sources of radiation are energetic particles, which are specifically electrons, protons, photons, alpha particles and heavy ions. When a material is struck by a particle the mass, charge, and kinetic energy of the particles all play a role in how much damage is caused [48]. The two main forms of degradation are displacement and ionization. This thesis will only focus on degradation due to ionization damage.

Total ionizing dose (TID) uses the unit rad which is the energy absorbed per unit mass of the target material [50]. Many materials used in circuits have different rates at which electron hole pairs (ehps) are generated per rad. Table 1 compares GaAs a direct bandgap material commonly used in optoelectronic applications to silicon and silicon dioxide. The mean energy required to ionize a material is dependent on the materials bandgap energy.

| Material | Mean Ep (eV) | Density ($g/cm^3$) | Pair Density per rad ($pairs/cm^3$) |
|---|---|---|---|
| **GaAs** | 4.8 | 5.32 | 7E13 |
| **Si** | 3.6 | 2.328 | 4E13 |
| **$SiO_2$** | 17 | 2.2 | 8.1E12 |

*Table 1 Relationship between ionization energy, density, and generated ehps [50]*

This leads to a strong relationship between bandgap energy and number of ehps generated at a certain dose.

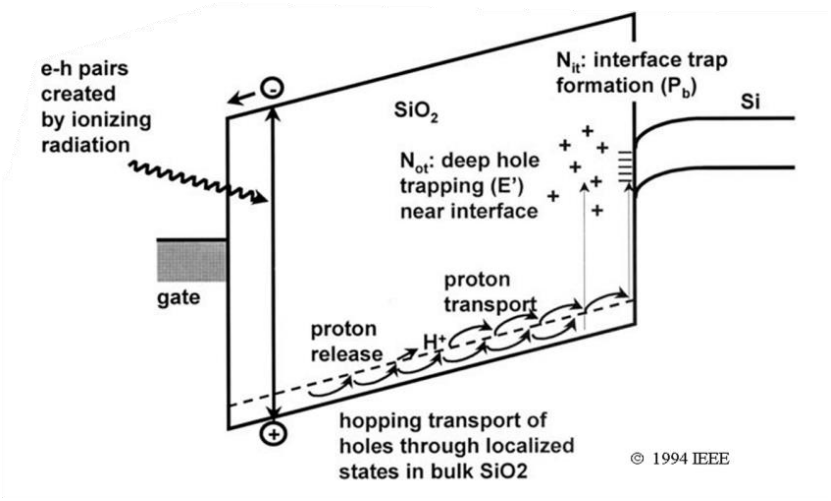


*Fig. 4 TID Damage Process [50]*

The process associated with TID damage in $SiO_2$ are shown in Fig. 4. These processes include 1) the generation of ehps, 2) recombination of some of the ehps, 3) transport of free carriers remaining in the oxide, and 4) creation of trapped charge in the oxide or traps forming at the oxide semiconductor interface [50]. The free carriers causing the oxide trapped charge and interface traps will be the focus for the remainder of the section.

Due to mobility differences electrons can move rapidly out of the oxide whereas holes have a much higher susceptibility to be trapped in the oxide. Hole mobility depends on the electric field and temperature. At low temperatures and low electric fields holes move slowly within the oxide [51]. The oxide trapped charge is typically net positive due to the slower holes being captured at oxygen vacancies within the $SiO_2$. There are two vacancy defects (E'): $E_\delta$' and $E_\gamma$'. The $E_\delta$' vacancy forms shallow traps within the $SiO_2$ bandgap energy around 1eV above the valence band. These shallow vacancies will allow holes to hop through the oxide. The $E_\gamma$' center is a deep trap at energy levels approximately 3eV above the $SiO_2$ valence band. Most of these defects are located near the

$Si/SiO_2$ interface [50]. Depending on their distance from the interface both defects are capable of exchanging charge with the Si layer. $E_\gamma$' centers located over 3nm away from the interface may capture and emit carriers, but in most circumstances the trapped holes are regarded as fixed. These $E_\gamma$' defects containing the fixed charges are denoted as $N_{OT}$. The buildup of this charge can be estimated by Eq. 3 [50].

$$\Delta \mathrm{NOT} = \mathrm{D}\,\kappa_g f_y f_{OT} t_{OX} \quad (1)$$

Where D is the TID level, $\kappa_g$ is the ehp density per rad, $f_y$ is fractional charge yield, $f_{OT}$ is the hole trapping efficiency, and $t_{OX}$ is the thickness of the $SiO_2$. These defects can alter surface potentials and carrier concentrations in underlying semiconductors, like silicon [48].

Interface traps ($N_{IT}$) are defects located exactly at the $Si/SiO_2$ interface. These traps have a very low barrier for trapping carriers, and therefore can drastically affect the carrier mobility and recombination rates at the surface of the semiconductor [50]. $N_{IT}$ is formed from reactions with $H^+$ ions drifting through the oxide to the semiconductor oxide interface. Campbell and Bogden reported experimental data which showed that under a positive bias almost all $H^+$ ions are converted into interface traps [51]. In dry gate oxides $N_{IT}$ formation does not depend on the oxide thickness, this points to the $H^+$ ions coming from the holes trapped near the interface as the main cause for $N_{IT}$ buildup. However, in wet gate oxides there is a lot of $H^+$ in the bulk of the oxide [48], [51]. Therefore, the way hydrogen is introduced during processing of the semiconductor plays a significant role in where holes will be trapped and where $H^+$ will be released. This influences the buildup time for $N_{IT}$ and

its dependence on oxide thickness [51]. The equation for formation of the defects can be seen in equation 4.

$$SiH + H^+ => D^+ + H_2 \quad (2)$$

The $D^+$ is the interface trap defect. This $D^+$ is a resulting dangling bond at the interface.

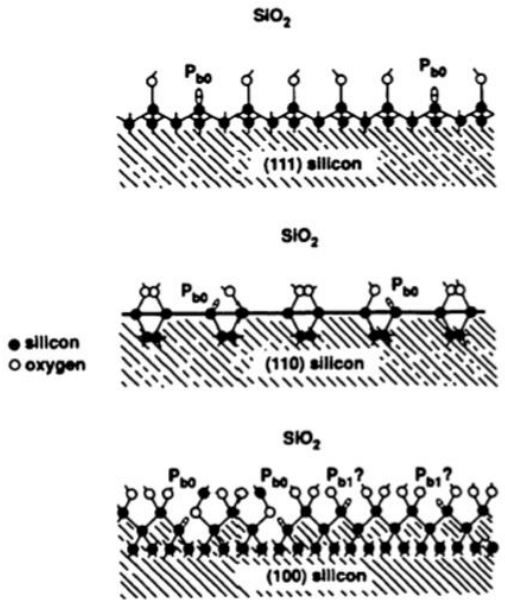


*Fig. 5 Interface Trap Defects for Different Miller Indices [50]*

In Fig. 5 from [50] $P_{b0,1}$ are both dangling bond defects caused by reactions with $H^+$ ions. In a bipolar process $N_{IT}$ buildup creates an excess base current due to the increase in surface recombination. Defects in semiconductors caused by TID cause shifts in key parameters, but the dose rate at which the irradiation occurs also plays a large role in degradation of a circuit.

### *2.2 Dose Rate Effects*

Dose rate (DR) effects also contribute to the degradation of semiconductors. Some CMOS processes (65nm, 130nm) have shown defects at certain TID levels within the

isolation oxides and the lightly doped drain spacers. These defects are similar to those generated within the passivation oxide layers of BJTs [52]. Dose rate dependent effects arise from reactions involving the electrons and holes in the semiconductor. At low dose rates (<0.1rad/s) these effects are nearly linear with the TID [36]. At high dose rates (>10rad/s) the larger carrier density in the oxide layers leads to more recombination or less carrier movement due to the electric field created by radiation generated charge [36]. Considering the defects due to TID ($N_{OT}$ and $N_{IT}$) the reactions involved when forming these defects play a critical role in determining the dose rate effects. First it is known that E' centers in the oxide trap the lower mobility holes. This can be modeled by Eq. 3 [36].

$$Trap^0 + p \rightarrow Trap^+ \tag{3}$$

At high dose rates the electron concentration is more notable which leads to the trapped holes being neutralized. A similar phenomenon can be seen in the $P_b$ dangling bonds from $N_{IT}$ [36]. Most of the dangling bond defects are passivated by hydrogen during processing and do not cause recombination [36]. Hydrogen released in the oxide moves to the interface and reacts with these bonds. From the previous section an $H^+$ is released when a hole is trapped at a hydrogenated defect in the oxide bulk. At high dose rates an electron can recombine with this hole before an $H^+$ proton is released [36]. This suppression in $H^+$ ion release reduces $N_{IT}$ buildup at high dose rates in bipolar oxides where the local electric field is low. Carrier trapping and recombing due to bimolecular recombination is the primary result in a high dose rate suppression, which explains the difference between high dose rate (HDR) and low dose rate (LDR) effects in BJTs.

LDR irradiation cause failures at far lower TID levels than HDR [6-9], [14], [17-23], [26-29], [36-43], [52], [53]. This concept is known as enhanced low dose rate sensitivity (ELDRS). Although MOS transistors are not typically subject to LDR failure there have been experiments which show dose rate dependencies at ultrahigh TID levels [52]. At low dose rates there is a faster buildup of $N_{IT}$. This is because at low dose rates the holes generated in the oxide are more likely to transport to hydrogenated-site and release $H^+$ proton that subsequently depassivate interface bonds and create interface traps. At higher dose rates holes can be confined by space charge which retards transport and makes recombination with electrons more likely. This reduces the amount of $H^+$ able to drift to the interface to create the $N_{IT}$ dangling bonds [36]. This can be seen in Fig. 6 [36]. The data shows that at low dose rates the $N_{IT}$ level is maximized and that the hydrogen impact saturates.

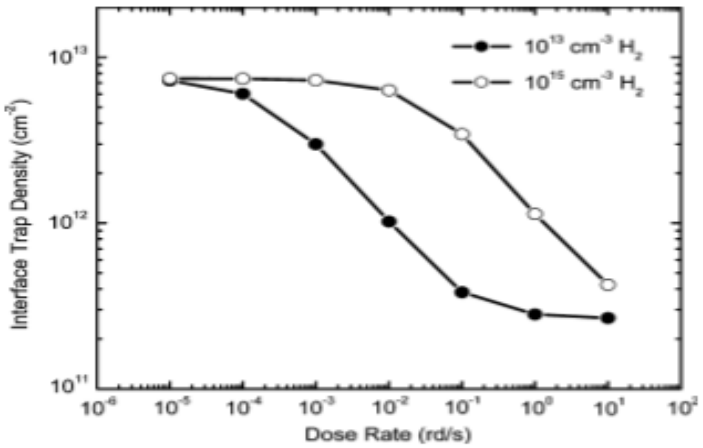


*Fig. 6 $N_{IT}$ Dependence on Dose Rate for Different $H_2$ Concentrations [36]*

*2.3 Total Dose and Dose Rate Effects on Bipolar Junction Transistors, both NPN and PNP*

Bipolar junction transistors (BJT) are the focus of this thesis since they are the transistor types used in the bandgap references studied here. BJTS exhibit significant TID and dose rate dependencies. Much research has been done on dose and dose rate (DR) effects in BJTS and there are many results showing BJTs sensitivity to both TID and DR. Some but not all BJTs experience ELDRS [6-9], [14], [17-23], [26-29], [36-43], [52], [53]. Radiation sensitivity is often attributed to the way the transistors are processed, biased, and their layout [18]. The base current of BJTs can drastically increase with little to no change in collector current. The excess base current $\Delta I_B$ caused by radiation leads to gain degradation in the transistor [6-9], [17-23], [31], [32], [34], [47]. This excess base current comes from the increased carrier recombination rate at the interface traps ($N_{IT}$). Radiation effects also increase the positive trapped charge within the oxide ($N_{OT}$) which is another factor contributing to the excess base current response [18], [21-23]. The remainder of this section will explore radiation degradation in both PNP and NPN transistors.

Lateral PNP (LPNP) transistors are commonly preferred for their flexibility and the simplicity of their fabrication. A lateral PNP BJT can be used as input stages, current sources, or active loads [34]. The LPNP transistor is of interest, because it has been shown to fail far earlier than NPN and vertical PNP transistors at low dose rates [20], [34]. These transistors fail due to losing their current gain ($\beta = I_C/I_B$). With the $I_B$ increasing due to an excess base current and the $I_C$ having negligible change the current gain factor goes down. The increased $N_{IT}$ levels cause more recombination on the $Si/SiO_2$

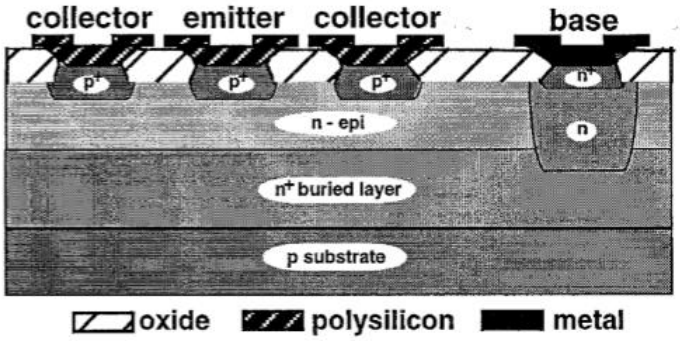


*Fig. 7 Lateral PNP Cross Section [34]*

interface which increases the recombination velocity at the surface of the base of the LPNP [20], [22], [34]. This then increases the recombination in the base region which leads to a base current increase [34]. However, in PNP BJTs, the $N_{OT}$ in the oxide reduces the amount of surface recombination as the surface recombination velocity increases. Holes trapped in the oxide create an imbalance between the two carrier concentrations which leads to less recombination at the base surface. Therefore, for PNP BJTs, the effects of $N_{OT}$ and surface recombination velocity oppose each other [34].

Ionizing dose damage most commonly occurs in oxides at the oxide semiconductor surface. This poses an issue for LPNP devices since their current moves across the surface near the semiconductor oxide interface [20]. Dose rate dependencies can be significant in LPNP BJTs. The ELDRS effects can be observed in the experimental data from [22] below which demonstrates a higher excess base current at low dose rates.

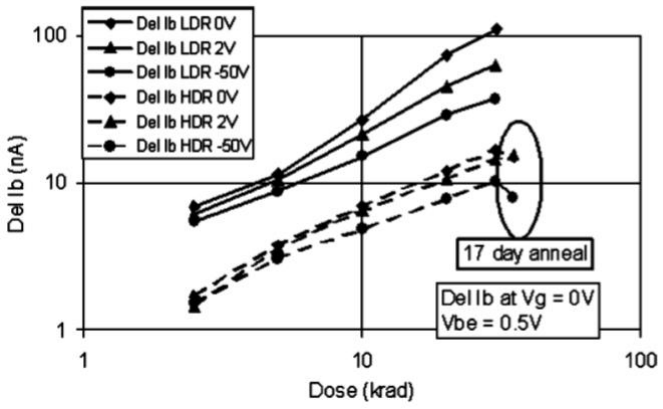


*Fig. 8 LPNP Excess Base Current Vs TID for different dose rates [22]*

Another point of interest is that annealing the wafer can reduce the excess base current at high dose rates. Thus, a true dose rate effect should consider the HD response after annealing over the same time as the LDR exposure. True dose rate enhancement factors aid in visualizing $\Delta I_B$, $\Delta N_{OT}$, and $\Delta N_{IT}$. The dose rate enhancement factor is essentially a ratio of the LDR response to the post anneal response of HDR. At low dose rates the $\Delta N_{OT}$, and $\Delta N_{IT}$ increase to much higher levels than those at low dose rates. The enhancement factor being a larger number indicates that the part exhibits greater low dose rate sensitivity [22]. Although not all LPNP transistors experience these ELDRS effects it is important to understand these worst-case conditions when considering their applications in space.

NPN transistors show less sensitivity than LPNP transistors for both TID and dose rate effects [8], [20], [22], [31], [34]. Like the LPNP transistors, the NPN transistors lose current gain due to increased surface recombination velocity, i.e., $N_{IT}$ buildup, causing an excess base current [31]. Within an NPN the oxide trapped charge depletes the base of the transistor an increase in the depletion region width where the maximum recombination occurs. For this reason, $N_{OT}$ is also a factor in increasing the base current of an irradiated

NPN [31]. This is opposite to the LPNP transistors where $N_{OT}$ mitigates the impact of $N_{IT}$ buildup and increased surface recombination velocity. NPN transistors show less dependence on dose rate effects. Below Figs. 9 and 10 show the same NPN transistors simulated with high and low dose rates respectively.

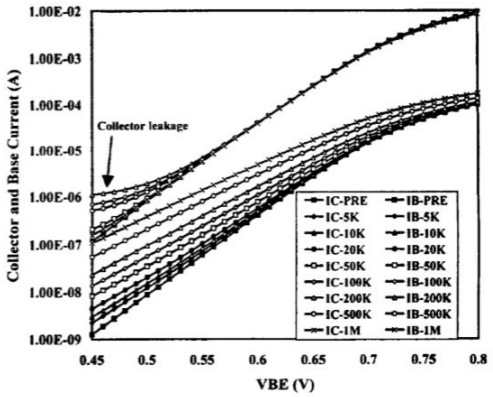


*Fig. 9 NPN transistor at HDR for different TID levels [8]*

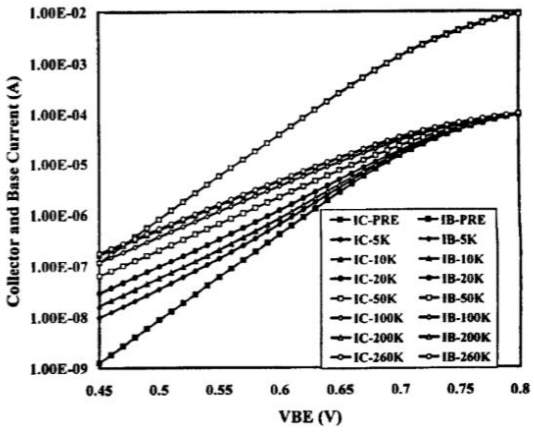


*Fig. 10 NPN transistor at LDR for different TID levels [8]*

These data [8] suggests less of a dose rate dependence in NPN devices. For most bipolar circuits NPNs and LPNPs are used in conjunction with one another. In operational amplifiers for example, LPNPs are typically used as input stages so that NPN may be used as gain stages. This can sometimes help circuit ELDRS due to the NPN transistors suffering

less degradation at low dose rates [34]. The following section will cover commercial-off-the-self-parts (COTS) containing both NPN and PNP transistors to compare their performances and identify critical transistors that impact radiation reliability.

*2.4 Radiation in Commercial off the Shelf Products*

Bipolar linear circuits used in COTS are of great interest when it comes to radiation hardness. Some COTS can have less radiation sensitivity based on their design. Studying these parts gives insight into the radiation sensitivities that different bipolar topologies experience. This section will focus on COTS low dropout regulators (LDO) due to their dependence on bandgap references (BGRs). Most LDOs use three blocks: BGR, Error Amplifier, and a pass transistor. The BGR sets the common mode input reference for the error amplifier. The error amplifier drives the pass transistor and uses feedback to maintain its proper biasing. The pass transistor takes the supply voltage and has a set voltage drop across it which sets the output of the LDO. The goal of a voltage regulator is maintaining a constant output over a wide range of conditions. The ability to identify how each block contributes to the failure of an LDO with irradiation allows engineers to have better insight as to how these LDOS will perform in the space radiation environment.

The LM117 is an adjustable voltage regulator with a 1.2 – 37V output range and a 1.5A output current capability. There is a modified Brokaw cell BGR used in the LM117 which allows the reference voltage of the BGR to be adjustable. A study of the LM117 was performed at both HDR and LDR in [8]. It was tested over a dose rate range of 1-150rad/s with total doses of up to 1Mrad.

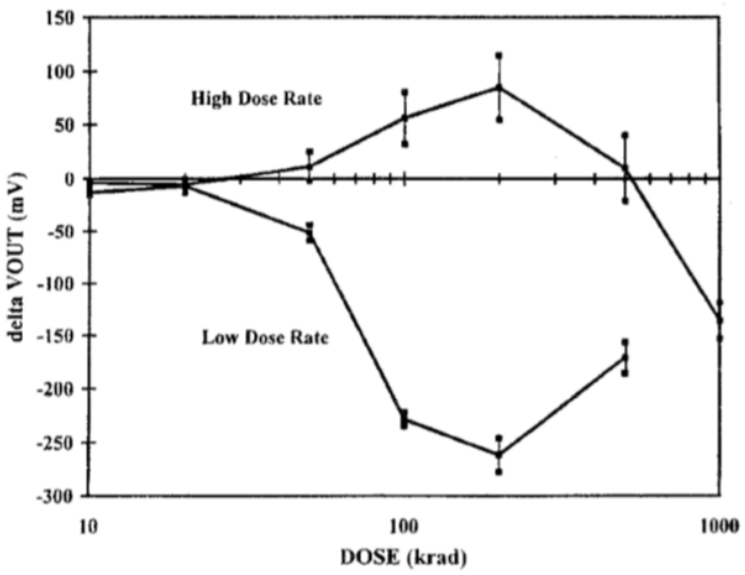


*Fig. 11 LM117 Output Voltage at HDR and LDR [8]*

When irradiated during high dose rates the output voltage increases before turning to a large negative slope at about 200krad. At low dose rates the output voltage decreases before turning back to a positive slope at about 200krad [8]. It was determined in [8] that this regulator response was a function of the BGR's reference voltage degradation. Critical transistors within the BGR were simulated in [8] to see if their behavior concurred with what was seen at the output of the regulator. The BGR's reference voltage followed a similar behavior as the output of the LDO at a high dose rate [8]. To build the model for the BGR its critical NPN and PNP transistors were characterized. At high dose rates the collector-emitter leakage current in the NPN transistors (Fig. 9) creates an increase in the reference voltage, however after 200krad the excess base current begins to dominate and decrease the reference voltage [8]. This agrees with the high dose rate output voltage seen in LM117 since the output voltage is dependent on the BGR's reference voltage. At low dose rate the decrease in output voltage is due to there being no collector emitter leakage

and only increased base current. For the LM117 the BGR is the main cause of total dose and dose rate dependencies. Although the BGR is the main cause of total dose and dose rate failures in the LM117 this is not the case for every LDO.

The LP2953 is a voltage regulator studied extensively for its total dose and dose rate sensitivity in [9], [12], and [18]. When tested at both high and low dose rates the reference voltage of the circuit was shown to drift in a similar pattern to the output voltage [9]. However, for high dose rate the output voltage remained within specification beyond 100krad. When tested at a low dose rate the output stays within specification until it gradually falls out of spec by 30krad [9], [12], [18]. The LP2953 also shows early output voltage degradation at LDR when the output current is increased. The pre-irradiated output voltage is maintained up to 300mA. At low dose rates the output voltage of the LDO only maintained up to 100mA [18]. Although only small voltage shifts are seen it is crucial that LDOs maintain its exact rated output voltage precisely since it supplies many sensitive reference voltages for larger circuits.

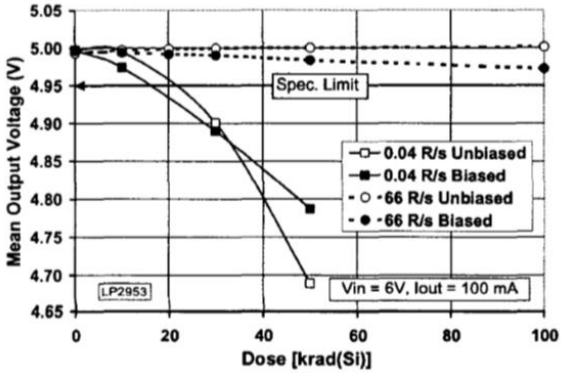


*Fig. 12 LP2953 Output Voltage over Dose for HDR and LDR [9]*

Fig. 12 shows the gradual degradation of the output voltage at LDR [9]. Although the shift is only from 0.2V – 0.3V at LDR this is more than enough shift to cause failures across a larger circuit. The LP2953's has an NPN bandgap reference which may explain its nonexistent HDR fluctuations and relatively gradual LDR changes. With the polarity of the BGR playing a role in the degradation of COTS it is important to compare the LP2953 to a PNP BGR to build a comprehensive understanding the radiation effects in a different BGR.

The LT1175 is a negative voltage regulator that can support 500mA of output current. The rated output voltage is -5V across the 0V to -20V supply range. The LT1175 maintains a constant output at HDR, but at LDR there is abrupt failure at total dose levels of 50krad or lower depending on the output current [9], [18]. Failures from the LT1175 show that the circuit loses its ability to drive the load [9].

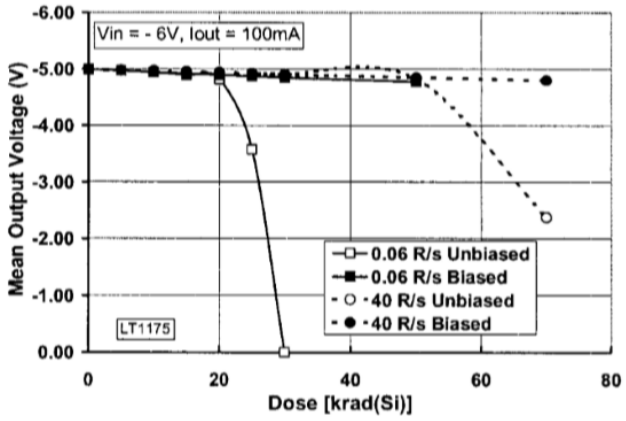


*Fig. 13 LT1175 Output voltage Vs Dose for LDR and HDR [9]*

The effects of ELDRS can be seen in Fig. 13 where the output voltage degrades much earlier at LDR than at HDR [9]. The more abrupt failure is attributed to the PNP based BGR design having a larger ELDRS effect than the NPN based design in the LP2953. The

LT1175 and LP2953 both show different dose rate dependencies especially at LDR. One major circuit differentiation comes from the BGRs having the opposite polarities in the two circuits. This will be shown to be the cause of the different failures. Chapter 3 will describe a solution to why BGR polarity affects the TID response, especially at low dose rates.

# CHAPTER 3 FAILURE ANALYSIS METHODOLOGY

## *3.1 Radiation Enabled Compact Models*

Bipolar transistors are comprised of two p-n junctions that can be controlled by three contacts. The base (B), collector (C), and Emitter (E). For example, a PNP transistor will have an n-type base with a p-type collector and emitter. The way these two junctions are biased controls how much or how little current passes through. Fig. 14 shows a simple diagram of a PNP BJT.

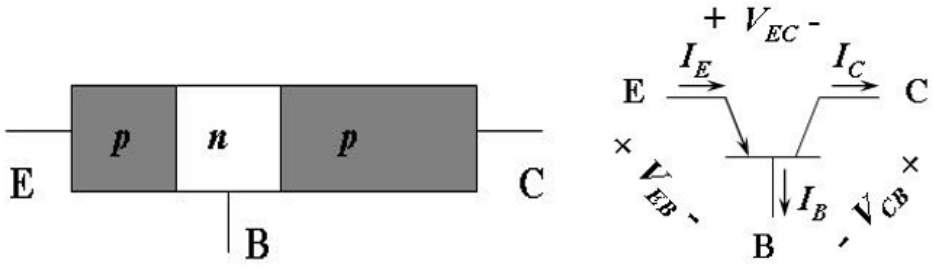


*Fig. 14 PNP transistor [54]*

BJTs have three main modes of operation: cutoff, saturation, and active mode. In cutoff there is no current flowing through the device. This is achieved by reverse biasing both pn junctions (for PNP BJTs, $V_E < V_B > V_C$). In saturation mode the transistor acts like a resistor based on $V_{EC}$ and both pn junctions are forward biased (for PNP BJTs, $V_E > V_B < V_C$). In forward active mode the base-emitter junction is forward biased, and the base-collector junction is reverse biased (for PNP BJTs, $V_E > V_B > V_C$). In active mode the transistor provides a constant current over all $V_{EC}$. A forward active BJT the current through the base ($I_B$) is much lower than the current through the collector ($I_c$). The ratio between these currents ($I_C/I_B$) is known as the current gain of the transistor (β) [54]. Radiation exposure

increases the base current of a BJT while only marginally increasing the collector current. This phenomenon causes current gain degradation and can be modeled in simulations by examining experimental data of BJTs.

BJT performance in a space environment can be modeled through simulation by using data collected from irradiated BJTs and fitting this data with compact models made in a simulation program with integrated circuit emphasis (SPICE). A test chip fabricated in a National Semiconductor process containing two gated controlled lateral PNP (GCPNP) BJTs, one LPNP BJT, and one NPN device was used for experimental data. The test chips came from a single wafer and were all given the same thermal treatments [18].

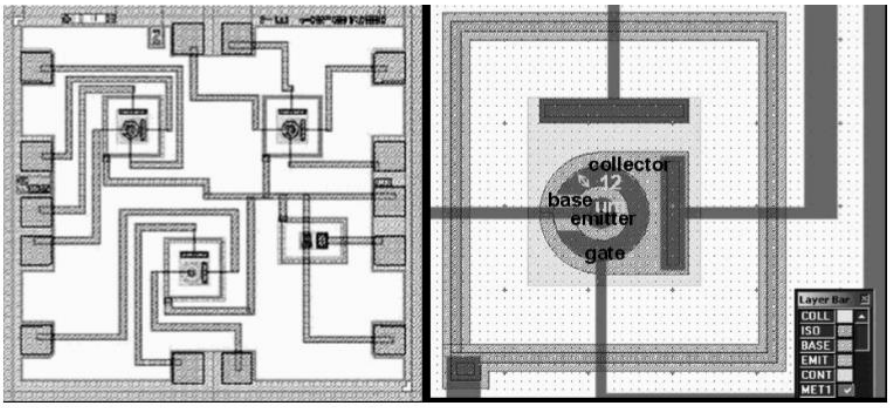


*Fig. 15 Left) Test chip full view Right) LPNP structure [54]*

NASA's jet propulsion laboratory (JPL) and Arizona State University both experimentally irradiated this test chip over a large variety of TIDs and DRs. After each irradiation step Gummel curves were created for the PNP and NPN transistors. This information was used to track the change in excess base current ($\Delta I_B$) from each step of irradiation. The change in the excess base currents were then plotted and a best fit was used to precisely model the effects.

The information gathered from the Gummel curves and best fittings enabled an accurate compact model design to be made. An accurate model of the $\Delta I_B$ can be made in SPICE by using a diode that is connected between the base and emitter of a BJT.

$$I = I_S * (e^{VD/nkT} - 1) \quad (4)$$

In Eq. 4 $I_S$ is the saturation current, VD is the voltage across the diode which is also equal to $V_{BE}$, and n is the ideality factor. By selecting different $I_S$ and n values the $\Delta I_B$ can be almost exactly matched for each case of experimental TID and DR level. By attaching this diode between each transistor in a SPICE simulator and adjusting the $I_S$ and n values respectively a simulation can be used to show radiation degradation. This is extremely valuable because it removes the need to experimentally test large amounts of parts because the simulation can be used instead. This can save a drastic amount of time and money when it comes to selecting parts for space missions.

*3.2 Reverse Engineering Commercial Off the Shelf Products*

The radiation enabled compact models grants the ability to simulate any circuit as if it had been irradiated. Using the compact models in a larger design gives an accurate prediction of a circuit's radiation sensitivity. By reverse engineering the COTS (LT1175 and LP2953) from chapter 2 the simulation data can be compared to the experimental data to verify that the compact models work on a larger scale. The LT1175 and LP2953 were reverse engineered using pre-irradiated compact models onto SPICE by matching a handful of the key parameters of the two voltage regulators to their respective datasheets. Specifications like the output voltage, supply current, output current, and input range were

all considered in the reverse engineering process. The following paragraphs will take a comprehensive approach to how each of the two regulators were reverse engineered.

The datasheet of the LT1175 has a handful of diagrams indicating potential structures used in the circuit. The target specifications were: $V_{OUT}$ = -5V, -5V < $V_{IN}$ < -20V, $I_{LOAD}$ = 0-500mA. The LT1175 uses a combination of two BJTs as a pass transistor, and error amplifier, and a BGR. After thorough examination the following block diagram of the LT1175 was accepted [18].

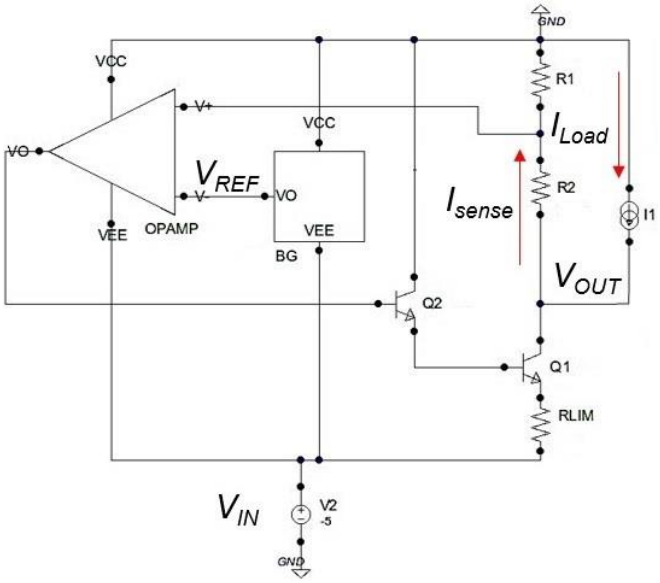


*Fig. 16 LT1175 Block Diagram [18]*

The BGR was specified to have an output voltage of $V_{REF}$ = -3.8V. The resistors R1 and R2 were used as a resistor divider to make the feedback of the error amplifier equal to the reference voltage

$$V^+ = V_{OUT} * \frac{R1}{R1+R2} \quad (5)$$

of the BGR. Since $V_{OUT}$ = -5V and it is necessary for $V^+ = V_{REF}$ = -3.8V the ratio between the resistors needs to be R1/R2 = 3.167. There is also a list of resistor dividers on the datasheet if an adjusted output is desired, but for this thesis a fixed -5V output is used. This ensures that the feedback to the amplifier will always match the reference voltage of the BGR. The focus of this thesis will be the BGR performance and therefore a simple differential amplifier was used that was able to properly drive the pass transistors. The bandgap reference uses a PNP output pair with a 1:10 current density ratio. This BGR needs a -3.8V output across the entire input range. With the different current densities and a resistor, a $\Delta V_{BE}$ is created between the two output transistors like the Brokaw cell from chapter 1.

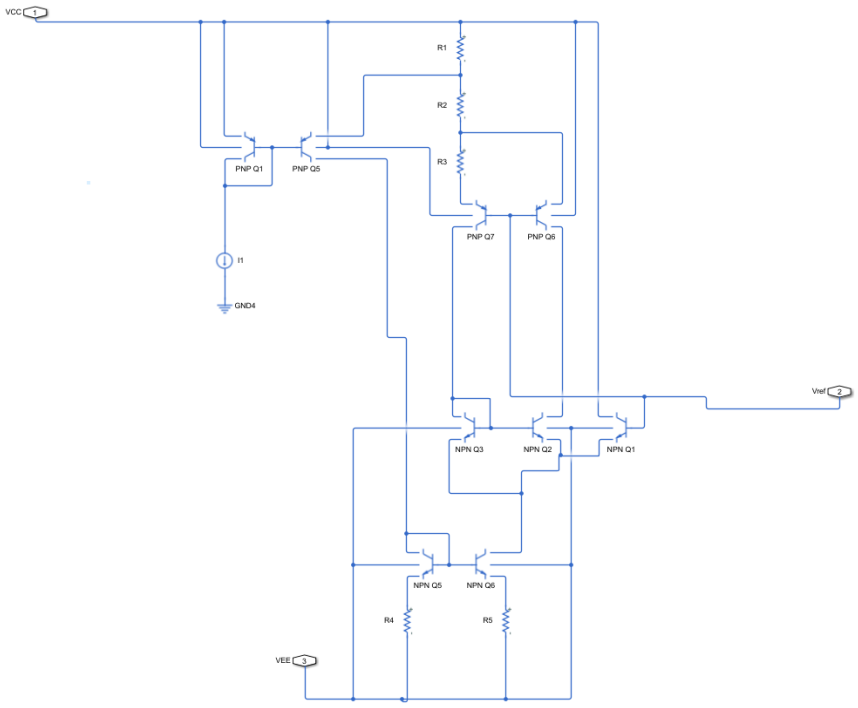


*Fig. 17 PNP Pair BGR for the LT1175*

Fig. 17 shows the BGR design implemented in the LT1175. With all the components of the LT1175 designed they can be simulated together and compared to the rated values. The reference voltage of this BGR along with the output of the reverse engineered LT1175 are shown in Table 2.

| | $V_{IN}$ = -5V | $V_{IN}$ = -10V | $V_{IN}$ = -20V |
|---|---|---|---|
| $V_{REF}$ | -3.64V | -3.76V | -3.96V |
| $V_{OUT}$ | -4.61V | -4.77V | -5.04V |

*Table 2 LT1175 BGR reference voltage and output voltage over the input range*

These values were obtained by simulating the circuit in Texas Instruments SPICE program TINA-TI. The reference voltage of the BGR stays mostly constant over the entire input range. The output of the reverse engineered LT1175 also shows near rated values over the input range. The small variations due to input range will be considered acceptable for this thesis. With the LT1175 operating properly as compared to the datasheet the LP2953 will be the next goal for reverse engineering.

The LP2953 is a positive low dropout regulator with an adjustable output voltage. For the sake of this thesis the output voltage target will be 5V across the input range. The input range for the LP2953 is 2.3V – 30V and the circuit can support 250mA of output current. The LP2953 has a similar structure to the LT1175 in that it contains a pass transistor, error amplifier, and a BGR. Looking through the LP2953's datasheet there are block diagrams describing the circuit, and the finalized diagram for reverse engineering is seen below. By controlling the resistor ratio, the common mode voltage of the amplifier

can be set to equal the reference voltage of the BGR. The properly biased amplifier can drive the pass transistor to have a proper voltage drop across it. The feedback for the amplifier will always provide the pass transistor the necessary bias to keep the LDO output at 5V. The BGR's reference voltage is stated as 1.23V in the datasheet.

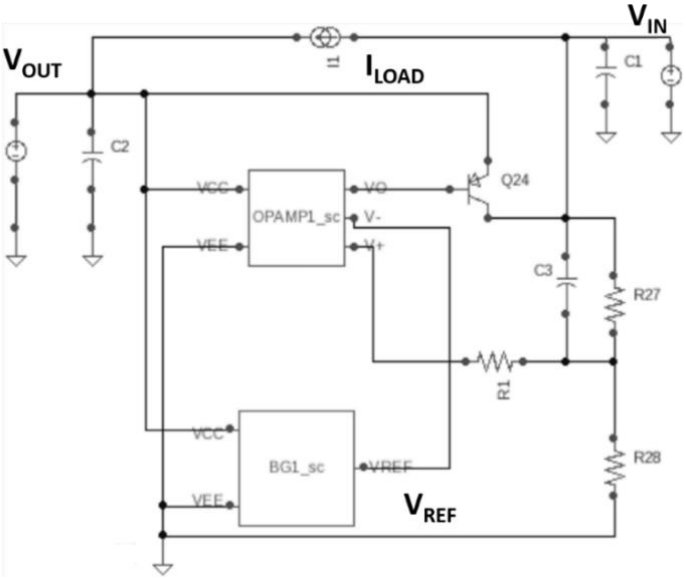


*Fig. 18 LP2953 Block Diagram [18]*

Again, the amplifier being used will be a simple differential amplifier so that the focus can remain the bandgap reference performance within the circuit. To remain consistent, the BGR being used in the LP2953 will have a similar topology as the LT1175 but with the opposite polarity. A 1:10 current density ratio is used in the two output NPN transistors. This causes a $\Delta V_{BE}$ between the two output transistors like the Brokaw cell. Looking at the Fig. above the $\Delta V_{BE}$ will be generated across the resistor R1. Since this thesis is using a 5V output fixed version of the LP2953 the input range is reduced to 5-30V. With this being stated Table 3 below shows the output voltage of the LP2953 and reference voltage of the BGR for selected values within the input range at 0A of output current. The simulation

program TINA-TI was used for the initial confirmation simulations. Both the BGR and LDO operate closely to the specifications of the datasheet. This performance will be accepted for the sake of this thesis. The LT1175 and LP2953 will now be able to be simulated as if they had been irradiated thanks to the compact models developed in part one of this chapter.

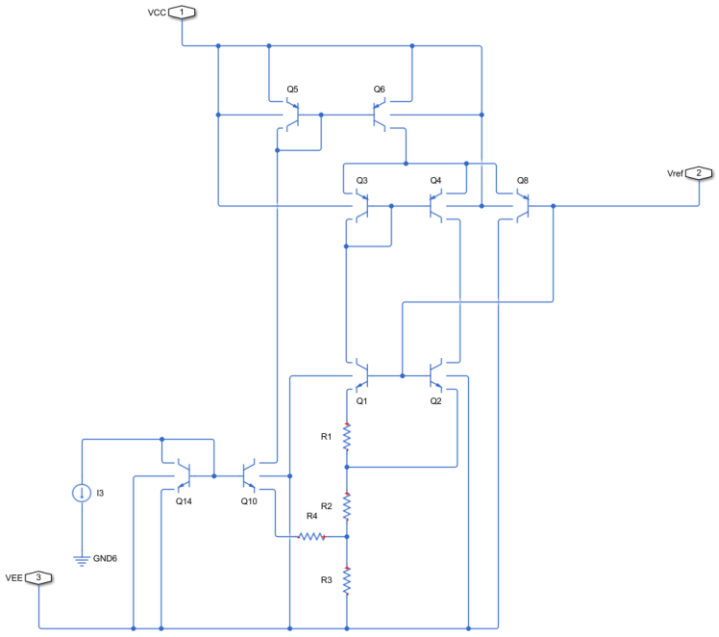


*Fig. 19 NPN pair BGR for the LP2953*

| | $V_{IN}$ = 6V | $V_{IN}$ = 30V |
|---|---|---|
| $V_{REF}$ | 1.22V | 1.24V |
| $V_{OUT}$ | 4.99V | 5.06V |

*Table 3 LP2953 BGR reference voltage and output voltage over the input range*

*3.3 Failure Analysis Approach*

The large amounts of radiation experimental data on the LT1175 and the LP2953 from [9], [12], [18] will prove useful in confirming the radiation enabled compact models' accuracy. Since the compact models have been verified in part one to match an individual transistors radiation effects they will be used in the reverse engineered designs of the LP2953 and LT1175. By making this replacement of models the two regulators should be able to imitate the experimental data found in [9], [12], [18]. This will prove incredibly useful because it will make radiation effects highly predictable in circuits if they are first simulated with these models.

Once the LT1175 and LP2953 designs were finalized their netlists were extracted. In the netlists of the LT1175 and LP2953 the diode developed in in part one of this chapter will be inserted in between the base and emitters of each transistor. The diodes accurately model the excess base current of the both PNP and NPN BJTs. By attaching a diode to each transistor, it will effectively be like the entire circuit has been irradiated. Based off the experimental data provided from JPL and Arizona State University only certain conditions were able to be experimentally obtained. At a high dose rate of 100rad/s there is data available for 2krad, 5krad, 10krad, 20krad, 30krad, 50krad, 100krad, 200krad, and 300krad. At a low dose rate of 0.01rad/s there is only data for 2krad, 20krad, 50krad, 100krad, 200krad, and 300krad. Each TID level for both HDR and LDR requires a specific diode saturation current $I_S$ and ideality factor n. Each $I_S$ and n combination requires an individual diode. Additionally, since NPN and PNP transistors have different dose rate

dependencies they will require sperate diodes. Each diode model for an NPN or a PNP serves as an excess base current model for a specific TID level at either HDR or LDR.

The benefit of using the netlists of the LT1175 and LP2953 makes modifying the circuits easy. A circuits netlist is essentially a text representation of the circuit. The text connects all the circuit elements to their appropriate nodes. In the netlists the compact model diodes are added in between the base and emitter of every BJT in the netlist. At the end of the netlist the transistor models, and diode models can be defined by their key specifications. The diode model can simply be defined by its $I_S$ and n values. By using the netlists, the diodes can easily be added, removed, and modified within the circuits. Changing the diode values in the LT1175 and LP2953 netlists allows the simulation of HDR and LDR radiation effects to be simpler.

The final simulations of these netlists were all performed on XYCE. XYCE is a software that simulates, and stores specified output values in log files. When simulating at HDR and LDR a separate simulation was needed for each TID level. First it is necessary to simulate the entire LT1175 and LP2953 at HDR and LDR to see if the compact models on a large scale can match the experimental data obtained in [9], [12], [18]. Once the simulations match the experimental data for both regulators the compact diode models will be fully accepted as accurate in this thesis. Once the diode models are fully verified another major benefit of using the netlists to simulate the circuit is that removing the diodes from certain transistors is easy. This makes simulating only certain blocks of a circuit for radiation effects possible. This is not feasibly possible from an experimental standpoint. Specifically, the LT1175 and LP2953 will be able to be simulated as if only the BGRs been

irradiated. These simulations will grant access into how a BGR specifically causes failures in two different voltage regulators.

# CHAPTER 4 RESULTS AND ANALYSIS

## *4.1 Low Dropout Regulator Compact Model Verification*

To make a more positive conclusion about the compact models it is necessary to verify their performance in COTS. There is a large amount of experimental data that exists on both the LT1175 and the LP2953. Before any conclusions can be made, the compact models must follow a similar trend to the COTS post radiation experimental data. This section will simulate the compact models in the reverse engineered LT1175 and LP2953 developed in the previous chapter. This simulation data will show slight short comings, but similar degradation behavior to the actual COTS experimental data.

The LT1175 LDO experimental data presented in Chapter. 2 shows the output voltage having little to no change at HDR and abrupt failure at around 30krad for LDR [9], [18]. Both sources indicate the LDO loses its ability to properly drive the current load at LDR. Simulating the reverse engineered LT1175 with the radiation enabled compact models should yield similar output failure mechanisms. Once reverse engineered LT1175 meets datasheet specifications on TINA-TI it's netlist is extracted. The radiation enabled models are attached to each transistor in the netlist and it is then simulated on Sandia National Laboratories XYCE software. A sperate XYCE simulation for each TID level is run and compiled separate HDR and LDR curves. The reverse engineered LT1175 with the radiation enabled compact models does show a similar trend to the experimental data. The compact models only account for the excess base current in each transistor, but since this effect is the most dominant in BJT failure the LT1175 simulations are near enough to the experimental data to be considered valid. Fig. 20 below shows LT1175's output voltage at LDR and HDR for the XYCE simulated netlist and experimental data.

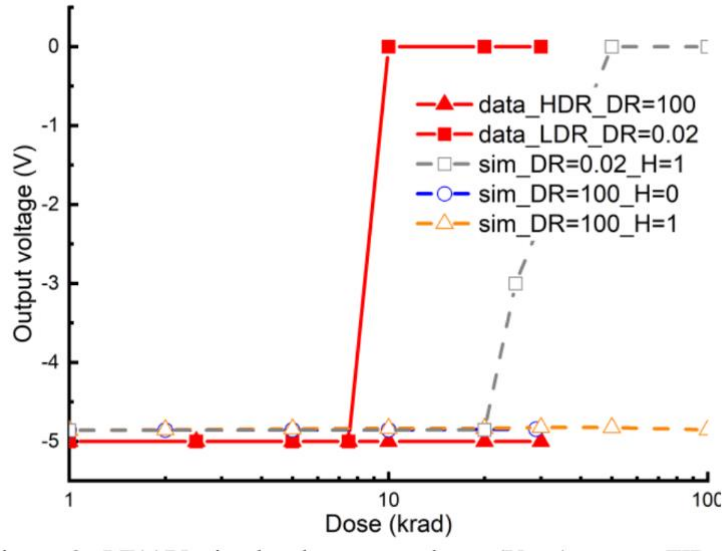


*Fig. 20 Experimental and Simulated LT1175 Output Voltage Plotted Against TID for HDR and LDR [18]*

The plot illustrates that the simulation data and experimental data for both HDR and LDR follow similar behaviors. For HDR the simulation and experimental data for the LT1175 maintain a -5V output across the entire TID range available for comparison. At LDR the experimental data fails abruptly at about 8krad where as the simulation data fails at 11krad. Although there is a slight difference in TID levels for the failures themselves are both abrupt. The netlist version of the LT1175 concurs with how the actual hardware LT1175 fails. With the LT1175 simulation agreeing with the experimental data this thesis will accept the netlist as a good representation of how the LT1175 will perform at HDR and LDR.

The LP2953 positive regulating LDO experimental data in Chapter 2 shows that the hardware maintains its output at HDR out to 100krad and does not show signs of failing. At LDR there is a more gradual failure starting at around 10krad. The output voltage

decreases by 4% of its value by 50krad. These experiments were done at 100mA of output current, and as the output current increases the failures begin at lower TID levels [9]. Fig. 21 below shows the output voltage of the LP2953 with 0A of current load and an input voltage of 2.3V.

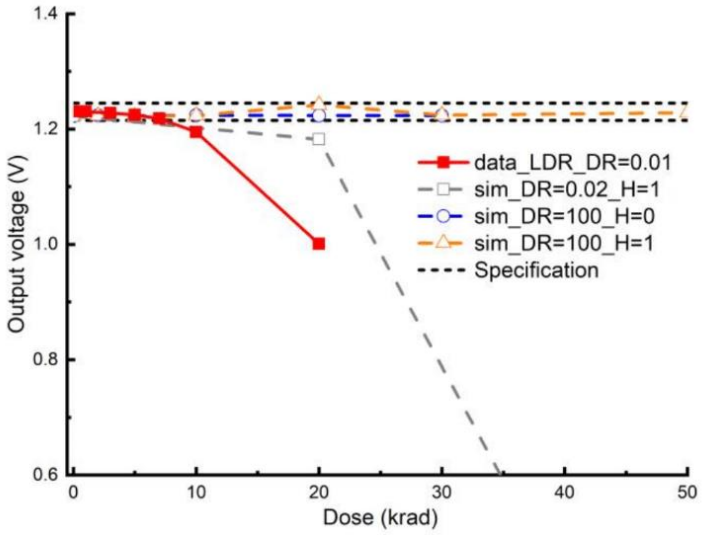


*Fig. 21 LP2953 Experimental data vs Simulated data for Output Voltage at $V_{in}$ = 2.3V and $I_{load}$ = 0A [18]*

Once again for HDR both the experimental data and the compact model simulation results both stay within spec for the entire TID range for which data is available. At LDR the experimental data and simulation show a gradual decay starting at around 10krad. The LP2953 also had data looking at the output voltage vs the current load. The HDR and LDR plot for the reverse engineered LP2953 and actual hardware is seen below in Fig. 22.

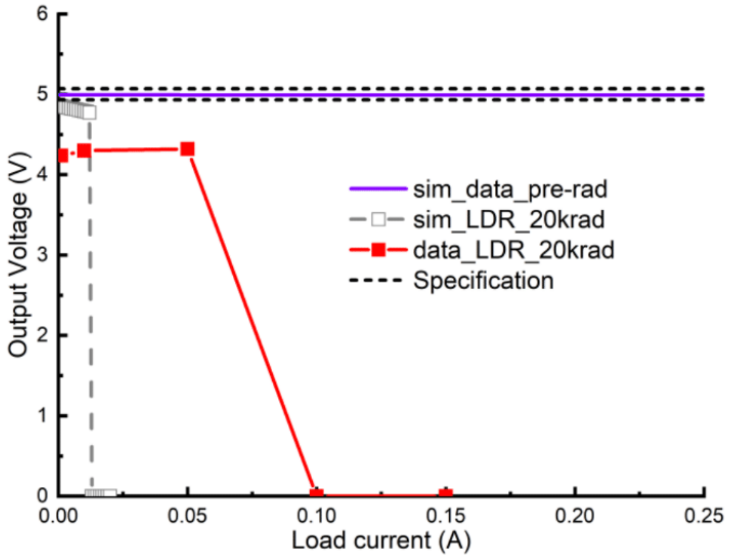


*Fig. 22 LP2953 Experimental data vs Simulation Output Voltage against $I_{load}$ at 20krad(Si) [18]*

The experimental data at 20krad of LDR has an out of specification output voltage for the entire output current range and fails quickly starting at 60mA. The reverse engineered LP2953 simulation circuit is slightly out of spec at 0 current and fails abruptly at around 10mA. Although the experimental data output voltage does not exactly match the compact model version of the LP2953 the rapid failure as current increases is a shared quality between them. The verification of the reverse engineered LP2953 is based more heavily on the experimental data and the simulation having a similar style of failure (i.e. gradual LDR failure against TID, and instant LDR failure as $I_{load}$ increases). The simulated version of the LP2953 and experimental data both fail in similar ways, and therefore the compact model version of the LP2953 will be considered as giving acceptable results for this thesis.

The compact models being used in the reverse engineered versions of the LT1175 and the LP2953 follow real post radiation experimental data. With the confirmed compact models both the LT175 and LP2953 can now be simulated as if their respective BGRs are

the only blocks being irradiated. Altering the netlist so that the compact models are only connected to the BGRs of the LT1175 and LP2953 will enable simulation of the LDOs as if only the BGRs have been degraded by radiation.

*4.2 Isolated Bandgap Reference Degradation in Low Dropout Regulators*

Simulating the LT1175 and LP2953 with only their BGRs degraded by radiation provides new information about specific radiation induced failures in the two LDOs. This simulated radiation isolation will assist in determining if the more prominent ELDRS effects in the PNP BGR are what causes the more abrupt failures in the LT1175. The two BGRs have reverse polarities but similar topologies. This consistency makes sure that the reference voltages of the BGRs depend on similar sources.

The LT1175 was shown to have abrupt failures at LDR in the compact model simulation and in the sources [9], [18]. The PNP BGRs contribution to the LT1175 failures may explain the reason the circuit fails abruptly compared to the more gradual decline of the LP2953.

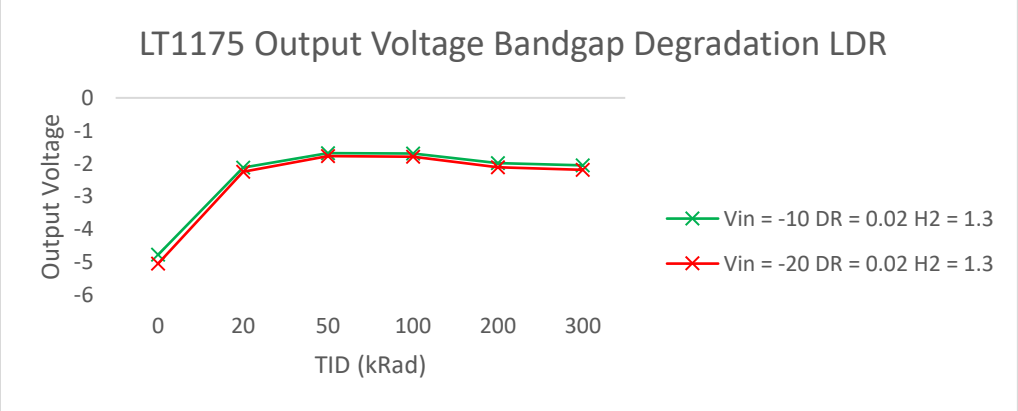


*Fig. 23 LT1175 Output Voltage with only the BGR Degraded at LDR*

Fig. 23 above shows the LDR responses of the LT1175 with only the BGR being degraded for a -10V and -20V input supply level. At LDR the LT1175 degrades similarly with the entire circuit irradiated and just the BGR irradiated. The LDO output voltage fails immediately and is fully dysfunctional by 20krad. The abrupt failure seen at LDR follows a similar pattern compare to when the entire LT1175 was irradiated in simulation and the experimental data from [9], [18]. This simulation points to the BGR of the LT1175 being the main source of failure for the LT1175 at LDR since data follows the same failure trend as the data in the previous section. The ELDRS effects in the PNP BGR seems to be the dominant force in the entire LT1175s failure at LDR. When considering the LT1175's ability to maintain its performance over the load current the PNP BGR is also the primary factor in degrading the output voltage. Simulations isolating degradation to the error amplifier and pass transistor do not make the LDO fail as early as the BGR does. This means that for the negative voltage regulator LT1175 the BGR is the main cause in output voltage degradation.

The LP2953 has an NPN BGR and it was shown in Chapter 2 that NPN transistors often experience less TID and ELDRS effects than PNP transistors. However, simulating the LP2953 with just its BGR irradiated will give insight as to how much the BGR influences the LDOs output behavior. From the previous section it is seen that experimental data and simulation data both show that the LP2953 has a more gradual degradation at LDR than the LT1175 [18]. The simulation of LP2953 with only its BGR degraded can be seen in the figure below.

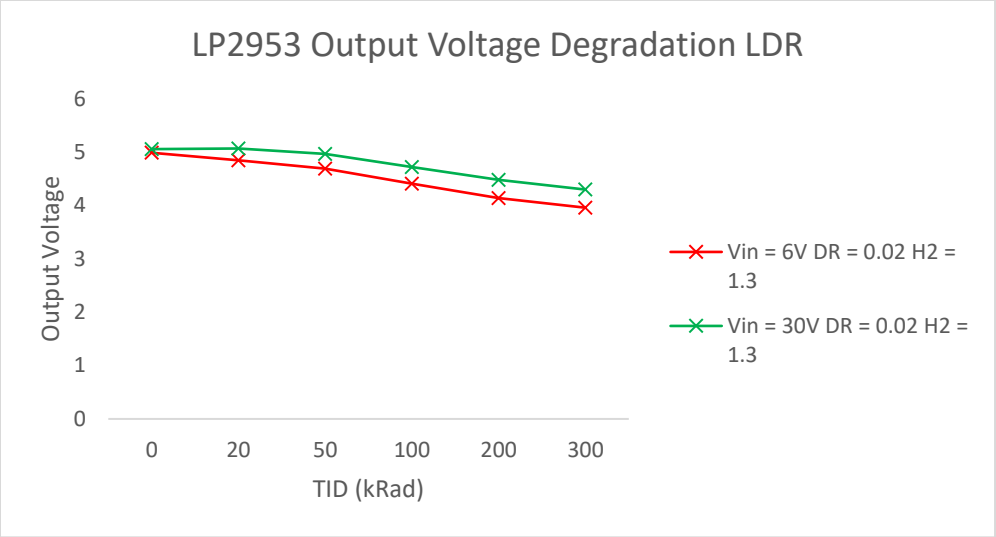


*Fig. 24 LP2953 Output Voltage with Only the BGR Degraded at LD*

The output voltage of the LP2953 with only the BGR irradiated shows a gradual decline over the TID range. This behavior is not comparable to the experimental data and simulation data from the previous section. With only the NPN BGR degraded the LP2953 stays within specification with little degradation. The experimental and simulation data above show the LP2953 falling out of specification at around 20krad. The NPN BGR does not cause the LP2953 to fail in this way. This points to the NPN BGRs lower degradation not being the main cause of failure in the LP2953. The error amplifier or pass transistor may be causing the failure in the LP2953. Since NPN BJTs experience less ELDRS effects than PNP BJTs it is expected that the BGR in the LP2953 performs better at LDR. The LP2953 was also unable to drive the current load in the experimental data. This simulation was also performed with only the BGR of the LP2953 being degraded.

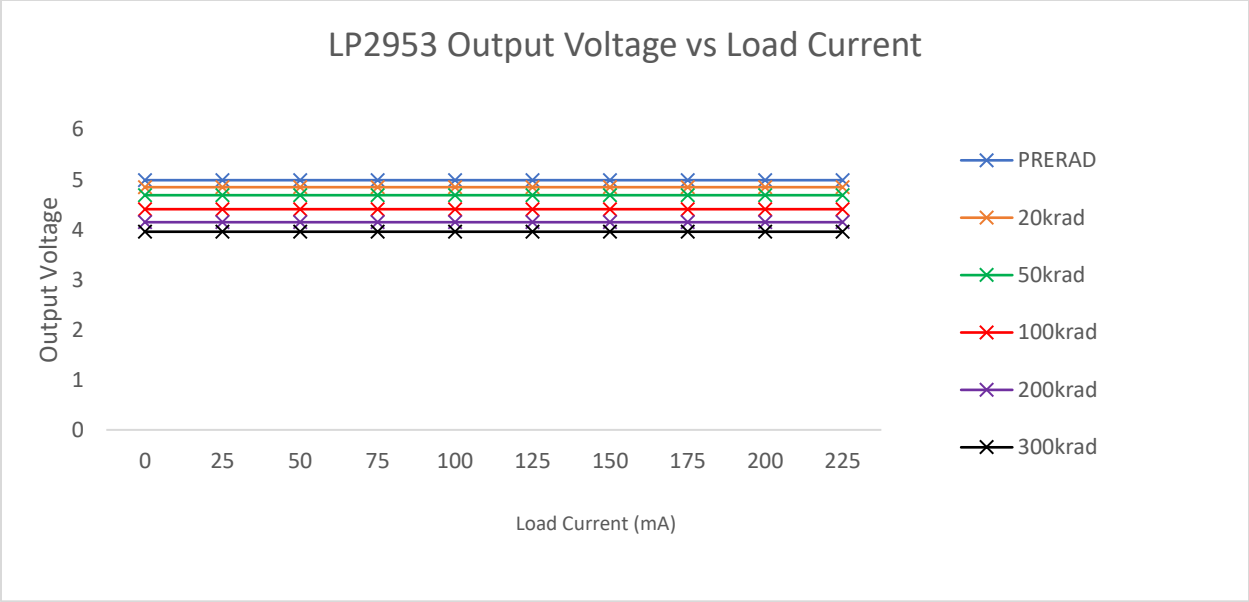


*Fig. 25 LP2953 Output Voltage Vs Load Current with only the BGR Degraded*

There is only a gradual output decay as the load current is increased in the LP2953. This is opposite to what the experimental data shows. The experimental data at LDR shows the output voltage failing abruptly once $I_{Load}$ > 10mA [18]. This simulation points the BGR not being the cause of the LDOs not being able to drive a load current at LDR. This means that the error amplifier or pass transistor are the cause this failure in the LP2953. Further investigation revealed that the pass transistor of the LP2953 causes the degradation of the output voltage due to the current load. Fig. 26 shows the output voltage of the LP2953 vs the load current with only the pass transistor degraded at LDR. The pass transistor in the LP2953 is a PNP BJT and this device's excess base current leads to the pass transistor not being able to properly operate and manage the rated load current.

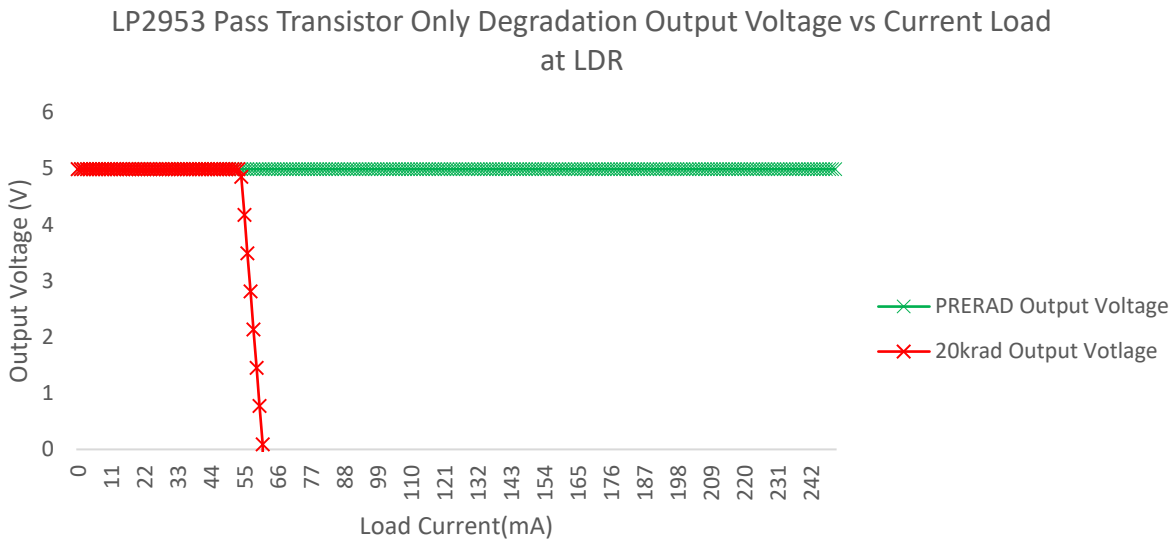


*Figure 26 LP2953 Output voltage vs load current*

The correlation between output voltage and output voltage over a current load for the LP2953 reinforces the fact that NPN BGR is not the leading source of error in the circuit. The output voltage of the LP2953 seems to be highly dependent on the BGRs performance, but current load performance depends entirely on the PNP pass transistor in the LP2953.

The LT1175 PNP BGR causes abrupt failures in the LDO due to the increased TID and ELDRS effects seen in PNP transistors. The LP2953 has an NPN BGR explains the more gradual degradation at LDR because NPN BJTs suffer less from these radiation effects. The LT1175 BGR only simulation has a similar abrupt failure at LDR when compared to its experimental data. This means that either the PNP BGR is the main cause of failure or a trigger that causes the failure of the error amplifier. The LP2953 NPN BGR simulation showed gradual degradation out to 300krad. The experimental data for the LP2953 shows the circuit failing at around 20krad. This means that the NPN BGR of the LP2953 is not the main cause of failure in the LDO. The output voltage versus load current

simulation also had gradual degradation at LDR and confirmed that the NPN BGR is not the main failure source. The next section will simulate the BGRs used in the LT1175 and LP2953 as standalone circuits. This will reveal correlations between how the BGR failures contribute to the LDO failures at LDR.

*4.3 Standalone Bandgap Reference Radiation Simulation*

The results from degrading only the BGR in the LT1175 and LP2953 points to the BGR potentially acting as a trigger to induce failures. For the LT1175 only BGR degradation simulation, the LDO's output voltage followed a similar trend as the experimental data for the entire LDO. The key difference was that the experimental data showed abrupt failure at approximately 10krad and the simulation with only the BGR degraded had abrupt failure at approximately 20krad when exposed to LDR. The LP2953 had more noticeable differences between the experimental data and BGR only degradation simulations. The LP2953 fell out of specification by about 20krad at LDR in the experimental data whereas the simulation data showed hardly any degradation across the entire TID range. The section will simulate the BGRs used within the LT1175 and LP2953 respectively. These simulations will give telling visualizations of the relationship between the BGR reference voltage and the output of the LDOs.

The LT1175 experimental data and simulation data shows abrupt degradation of its output voltage at LDR [9], [18]. After isolating and simulating the circuit with only its BGR degraded this trend continued. The BGR of the LT1175 is specified to operate at a reference voltage of -3.8V. Fig. 27 below shows the BGR of the LT1175 simulated as a standalone circuit at LDR.

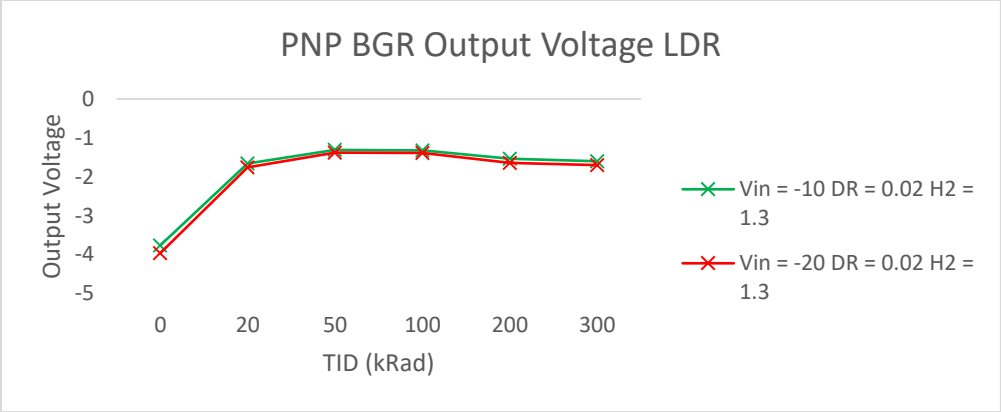


*Fig. 27 LT1175 Standalone BGR Reference Voltage at LDR*

The BGR starts at a proper reference voltage, but also abruptly fails by a TID level of 20krad. The failure of the BGR shows a directly proportional relationship to the failure of the LT1175 at LDR. The standalone BGR simulation data confirms that the BGR is the main cause of failure in the LT1175 at LDR for this methodology. To specifically isolate what was the cause of the failure in the PNP BGR a simulation at LDR was run with the goal of monitoring the voltages and currents of the interior nodes. Fig. 28 considers the $\Delta V_{be}$ formed across the critical 1:10 ratio transistors.

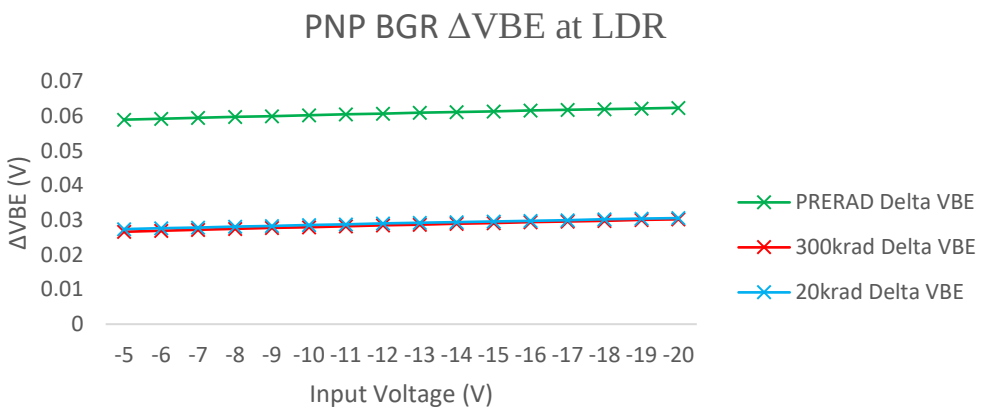


*Fig. 28 $\Delta V_{be}$ of the 1:10 Critical Transistors at LDR*

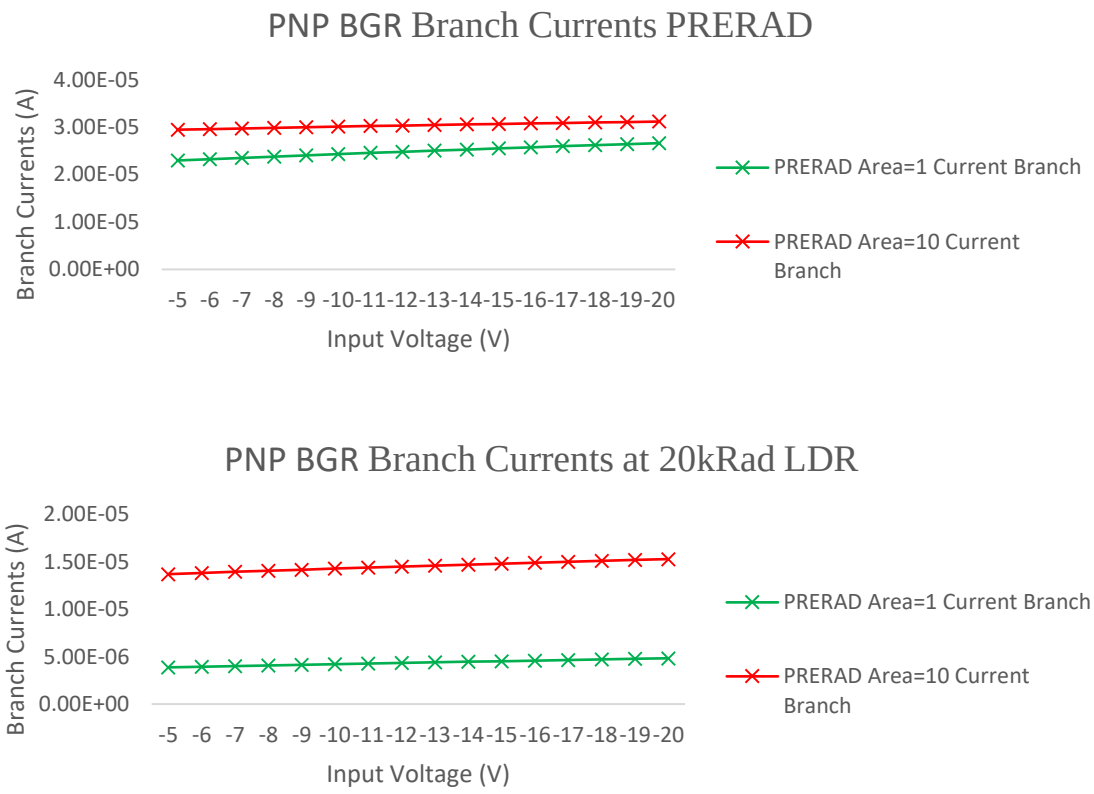


*Fig. 29 Currents down the 1:10 Branches Prerad (TOP) and 20kRad LDR (BOTTOM)*

Figs. 28 and 29 show the reasoning behind the PNP BGR's failure. The PNP BGR fails at 20krad and Fig. 28 shows that at 20krad at LDR the $\Delta V_{be}$ between the 1:10 transistors that is designed to be 60mV takes a 50% drop to 30mV. This $\Delta V_{be}$ is gained up and serves as a factor to set the reference voltage of the BGR. Additionally, the 1:10 transistors are meant to run at the same current which creates a 1:10 current density ratio through the BGR. Fig. 29 shows that at 20krad during LDR the currents between the branches degrades to create a 66% difference in current between the branches. This means that the branches are not running at a 1:10 current density ratio which therefore contributes to the failure of the PNP BGR at LDR. Although this specific simulation cannot be easily verified with experimental data it will be considered reliable in this thesis due to the consistency of the compact model

results to experimental data results for the entire LT1175. The PNP BGR in the LT1175 shows clear signs of TID and ELDRS effects. Since PNP transistors experience more degradation as seen in Chapter 2 these results abrupt failures due to TID ELDRS can be expected.

The LP2953 simulation data shows more gradual degradation than that of the LT1175 [9], [12], [18]. The LP2953 when only the BGR is degraded at LDR degrades the output voltage by 15% at LDR for the TID range (0-300krad). The experimental data shows output failure by 20krad at LDR. These results show that the BGR in the LP2953 may not be the quickest block to fail at LDR in the LDO. To further confirm this the BGR of the LP2953 was also simulated as a standalone circuit with the compact models developed in Chapter 3. The standalone BGR simulation for the LP2953 is shown in the figure below.

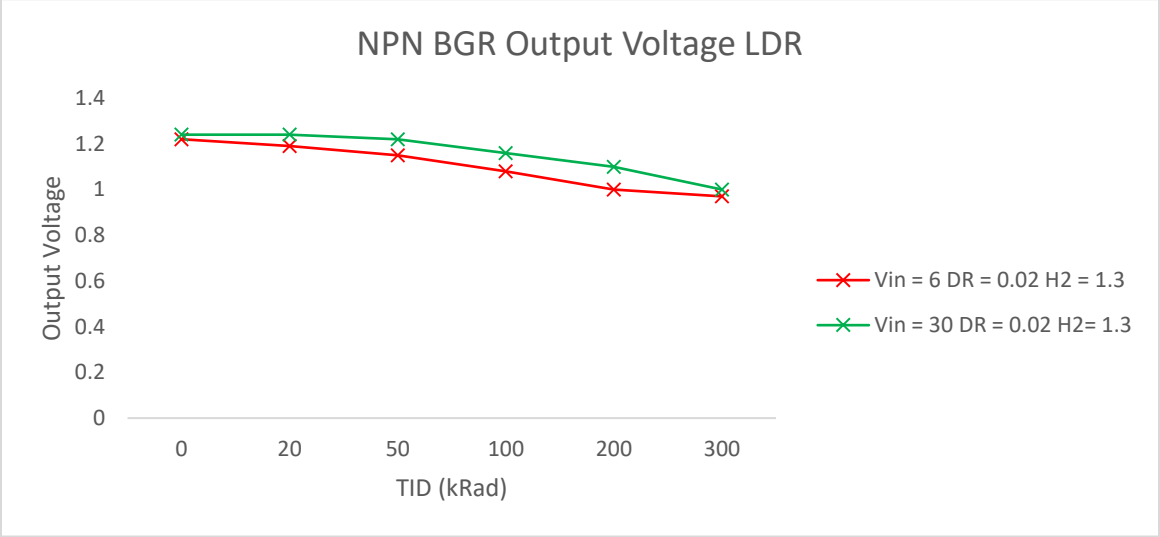


*Fig. 30 LP2953 Standalone BGR Reference Voltage at LDR*

The standalone BGR simulation data shows a directly proportional relationship to the output voltage of the LP2953 when only the BGR is degraded at LDR. The BGR starts

at its rated 1.22V reference and this degrades to 1V by then end of the TID range. This is an 18% degradation which is closely comparable to the degradation seen in the simulation results LDO with only the NPN BGR degraded at LDR. The NPN BGR has a proportional relationship to the output voltage of the LDO. However, there is no failure seen across the entire TID range which may mean that the NPN BGR is not the limiting block of the LP2953 at LDR. This can be attributed to the minor changes in the NPN BGR's internal voltages and currents. Figs. 31 and Fig. 32 shows the $\Delta V_{be}$ of the 1:10 transistors as well as the currents down each of the branches.

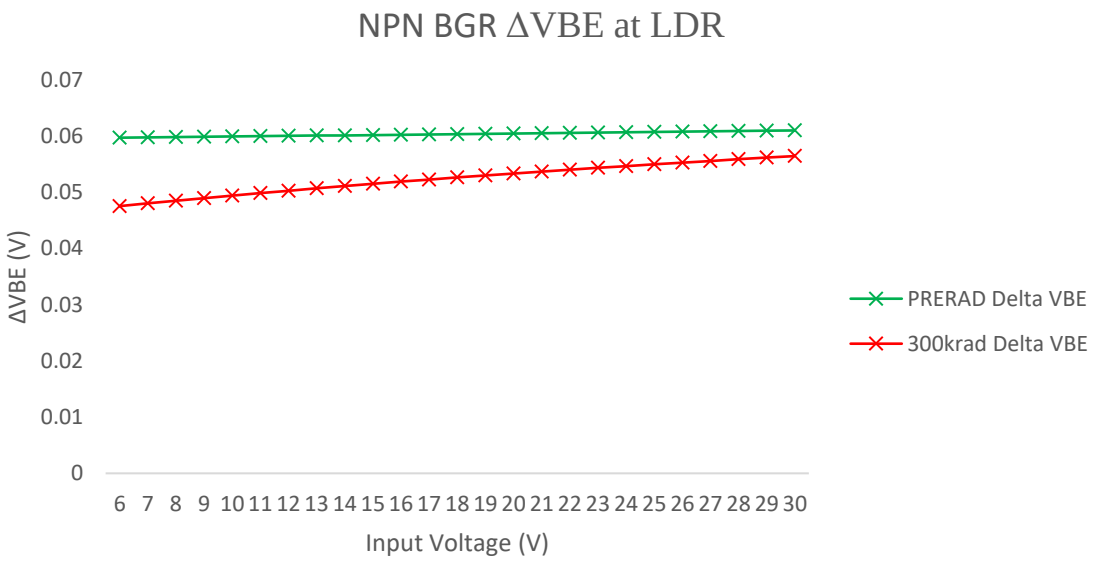


*Fig. 31 $\Delta V_{be}$ of the 1:10 Critical Transistors at LDR*

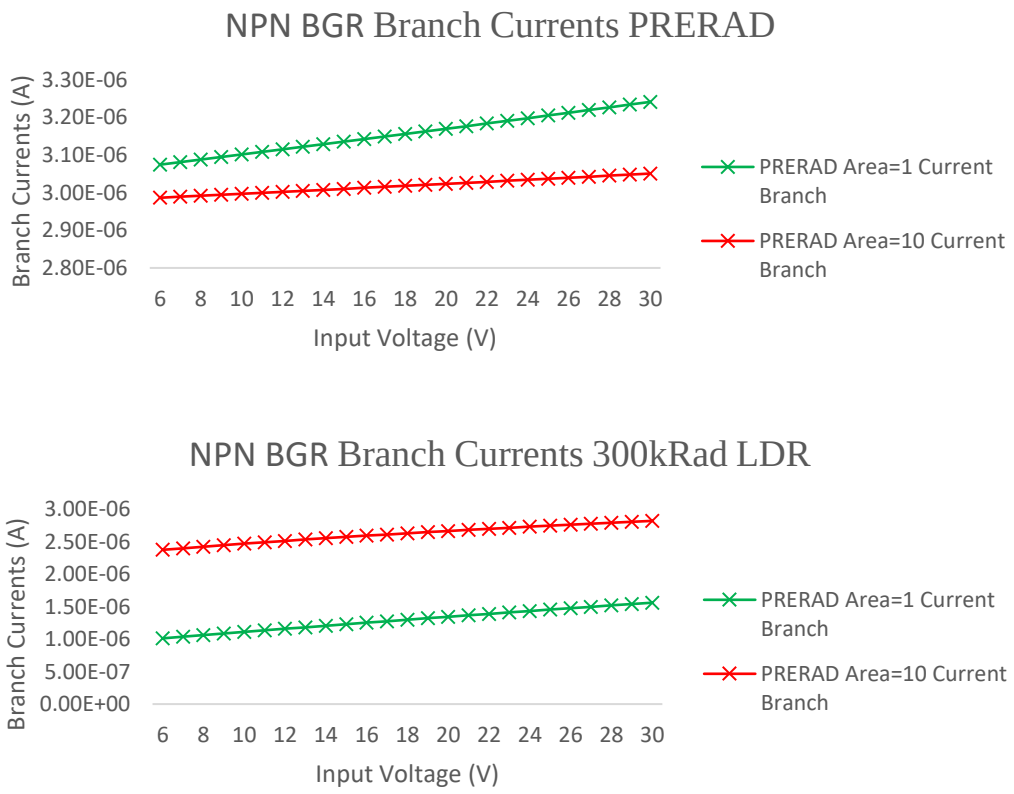


*Fig. 32 Currents down the 1:10 Branches Prerad (TOP) and 300kRad LDR (BOTTOM)*

From Fig. 31 and Fig. 32 there are only minor changes in the $\Delta V_{be}$ and currents through the 1:10 transistors. The $\Delta V_{be}$ changes by around 20% across the entire TID range at LDR. This degradation is reflected in the reference voltage of the BGR. The currents down the branches do change substantially, due to the excess base current introduced at 300krad, but the $\Delta V_{be}$ remaining mostly constant helps the BGR maintain its performance with only gradual degradation. The data presented in this section showed that the BGRs reference voltages of both the LT1175 and LP2953 have proportional degradation to the output voltages of the LDOs with only their BGRs degraded at LDR. A key result to observe is the PNP BGR of the LT1175 exhibits a much more abrupt failure than the NPN BGR of the LP2953. This could be due to the PNP BJTs experiencing more ELDRS effects

than the NPN BJTs. The BGR in the LT1175 could be the main cause of LDR failure in the LDO, or it could act as a trigger causing another block to fail. The NPN BGR in the LP2953 has little degradation across a large TID range at LDR which points to another block causing the 20krad failure seen in the experimental data. The next chapter will conclude on the results found in this chapter and provide suggestions about what polarity of BGR to select for applications in an environment where radiation threats exist.

# CAHPTER 5 CONCLUSION

## *5.1 NPN vs PNP Standalone Bandgap References*

Space exploration is on the rise; however, it proves to be a difficult environment for bipolar linear circuits to operate in. Analog/Mixed Signal (A/MS) circuits in space are exposed to constant radiation and they need to maintain their performance for a long lifetime. Specialized radiation hardened A/MS circuits can perform this function at a high cost. This thesis has proposed a method of quickly and cheaply assessing COTS products for their radiation hardness. This method of hardness verification led to the conclusion that NPN BGRs will have much more long-term reliability in an environment where radiation exists. The compact models enable the simulation of all COTS parts quickly at both HDR or LDR. This method can greatly decrease the time and money required to verify many COTS parts experimentally. This thesis focused on simulating the LT1175 and LP2953 with specific goals of comparing PNP and NPN BGR radiation robustness. Verifying that NPN BGRS have a gradual degradation at LDR compared to the PNP BGRS abrupt degradation can help design engineers quickly decide on what type of BGR may be the most useful in their application's needs.

Looking back at Chapter 2 experimental data shows that not all BJTs experience the same TID and ELDRS effects [6-9], [14], [17-23], [26-29], [36-43], [52], [53]. An LPNP BJT is more likely to exhibit these effects then an NPN BJT. [20], [34]. This is because in an LPNP the base current is more sensitive to surface recombination. This allows radiation induced defects like the dangling bonds of $N_{IT}$ to degrade the transistor. The compact models developed in Chapter 3 were created from experimental data taken on a test chip that had LPNP and NPN BJTs. The compact models implemented a diode

connected between the base and emitter of the BJTs to model their $\Delta I_B$. The $\Delta I_B$ in BJTs is the main cause of failure in a BJT due to it creating a large amount of gain degradation in the transistors [6-9], [17-23], [31], [32], [34], [47]. The failures seen in Chapter 4 in the LT1175 and LP2953 are due to the gain degradation of the BJTs. The LDR failures causing the BGRs to degrade stems from the degradation occurring in the critical 1:10 transistors in the BGR discussed in Chapter 1. These transistors have the same current flowing through each branch and due to their area differences, this means one branch is operating at 10X the current density of the other. This creates a $\Delta V_{be}$ (ideally 60mV) between the transistors that serves as a reference voltage of the BGR. In the PNP BGR this $\Delta V_{be}$ degrades 50% by 20krad at LDR. This degradation is the cause of the PNP BGR's reference voltage degradation. The NPN BGR sees about a 20% decrease in the $\Delta V_{be}$ across the entire TID range at LDR. This explains why the NPN BGR has only gradual reference voltage degradation across then entire TID range.

As seen in Chapter 4, the PNP BGR of the LT1175 has its reference voltage degrade by 73% by 20krad at LDR. The NPN BGR of the LP2953 had a reference voltage degradation of about 18% across the entire TID range at LDR. From these simulations the NPN BGR of the LP2953 is much more resistant to radiation damage at LDR than the PNP BGR of the LT1175. The PNP BGR reproduces TID and ELDRS effects due to the LPNP characteristics that the compact models were created from. The standalone BGR simulations for the LT1175 show similar methods of failure as the experimental results. The only difference is the abrupt failure occurs at 11krad in the experimental data and 20krad in the BGR degradation simulation. This signifies that the PNP BGR either is the main cause of the abrupt failure at LDR or a trigger to cause another block to fail. The

ELDRS effects causing the degradation of the BGR is likely most prominent in the 10:1 transistor ratio that creates the $\Delta V_{BE}$ within the BGR. From Chapter 1 a $\Delta V_{BE}$ is designed in a BGR by having a pair of transistors with a 10x difference in their corresponding current densities. ELDRS effects causing a $\Delta I_B$ in these transistors would cause one of the transistors to degrade 10x faster than the other. This explains the abrupt failure of the PNP BGR's reference voltage. The difference between the BGR only simulation and the experimental data of the LT1175 likely comes from the BGRs degradation causing a more rapid degradation in the error amplifier. The LP2953's NPN BGR degradation at LDR does not have comparable results to the experimental data from the entire LDO. In the simulations when the BGR is degraded only the output voltage of the LP2953 degrades a mere 18% across the entire TID range at LDR. The experimental data for the LP2953 has the LDO falling out of specification by 20krad. Comparing these results points to a different block being the cause of the LP2953's failures at LDR. With this information it can be concluded that the PNP BGR shows drastically more degradation at LDR than the NPN BGR. Future work can use the compact models to simulate more topologies of BGRs to verify if the results presented in this thesis are constant across all topologies. Extending this work into more BGR topologies will provide designer engineers with more at hand information to help them quickly decide what BGR is right for their specific application.

### *5.2 Bandgap Reference Contributions to Low Dropout Regulator Failure*

The BGR supplies a stable reference voltage for the LDO to operate on [1], [2]. This crucial circuit block is proven in this thesis to be a main factor in LDO failure due to radiation exposure. The $\Delta I_B$ introduced by radiation from $N_{OT}$ and $N_{IT}$ defects causes a shift

in the BGR's reference voltage [8], [9], [12], [14]. The BGR sets the common mode voltage of the error amplifier in the LDO. If there is a large enough drift the reference voltage will fall out of the error amplifiers common mode range and eliminate all functionality in the LDO. The simulation results found in this thesis by targeting only the BGR with radiation effects shows a clear correlation between the BGR reference voltage and the output voltage of the LDO's. However, when the positive LDO is simulated against its current load the NPN BGR is not the cause of the output voltage degradation. The loss of load current capabilities comes from the PNP pass transistor in the LP2953. In the negative voltage regulator, the PNP BGR still remained the earliest cause of failure due to the current loading.

Isolating the radiation effects to the BGR of the LT1175 and LP2953 shows a proportional relationship between the reference voltages of the BGRs and output voltages of the LDOs. After simulating the LT1175 and LP2953 with only their BGRs irradiated the results seen were slightly different when compared to the experimental data obtained by irradiating the entire part. For the LT1175 at LDR there was an abrupt degradation in the regulators output voltage of 80% by 20krad of TID. The experimental data shows the output voltage of the LT1175 degrading by about 10krad. This means that the PNP BGR degradation likely acts as a trigger to degrade the error amplifier of the LT1175 at a faster rate. This explains why the isolated BGR simulations fail at 20krad as opposed to the 10krad failure of the entire circuit at LDR. The LP2953 at LDR demonstrated 15% of degradation at the output voltage across the entire TID (0-300krad). However, experimental irradiation at LDR shows the LP2953's output voltage degrading out of spec

by 20krad. A more abrupt failure can be seen in the LP2953 when the PNP pass transistor is degraded and current load is swept. The LDO fails abruptly by 20krad and loses almost all its rated current load performance. Comparing the results of the LP2953 shows that the NPN BGRs little degradation is not the cause of the LP2953s degradation it is the PNP pass transistor. The results from both LDOs show that the ELDRS effects seen in the PNP BGR leads to the BGR having a more prominent role in the output voltage's degradation. The NPN BGR shows little TID and ELDRS effects which leads to the pass transistor as the main cause of the output voltage's degradation.

NPN and PNP BGRs have different responses when exposed to radiation most notably at LDR. This thesis has verified that LDR performance differences in the two types of BGR with a compact model simulation. The radiation enabled compact models were used in reverse engineered COTS parts (LT1175 and LP2953) and their results were comparable to the experimental data that they were developed from. The LP2953 contained an NPN BGR that showed gradual degradation at LDR over a large TID range. The results showed that the NPN BGR's minor degradation at LDR were not the main cause of the LDOs output voltage degradation. The main cause of the LP2953s output voltage degradation was the PNP pass transistor degradation. This caused an abrupt failure by 55mA of load current at 20krad of LDR. The LT1175 contained a PNP BGR and showed abrupt output voltage degradation at LDR. The LT1175's PNP BGR's LDR output voltage degradation shows comparable results to the entire LDO being irradiated at LDR experimentally. The radiation effects seen in the PNP BGR creates a trigger that causes the rest of the blocks within the LT1175 to degrade at lower TID levels. The NPN BGR's

minute degradation at LDR points to the NPN BGR having less total effect on the LP2953's output voltage degradation. The information found in this thesis will help design engineers quickly and easily decide on which LDO to use in space applications based on the circuit's BGR (PNP BGR acts as a trigger to cause failure at LDR and the NPN BGR does not). Selecting an LDO based on the BGR's polarity will greatly decrease the testing time and costs required because, it is easier to narrow down which LDOs will likely be able to perform properly in the application. Space exploration is gaining popularity and with the results presented in this thesis it will be possible to reduce time in part selection by using COTS LDOs based on the type of BGR they use.

# REFERENCES


[1] Gray, Paul R. Analysis and Design of Analog Integrated Circuits. 3rd ed., Wiley, 1993.

[2] Pease, R.A. "The Design of Band-gap Reference Circuits: Trials and Tribulations." *Bipolar Circuits and Technology Meeting, 1990., Proceedings of the 1990* (1990): 214-18.

[3] Kuijk, K.E. "A Precision Reference Voltage Source." *Solid-State Circuits, IEEE Journal of* 8.3 (1973): 222-26.

[4] Baker, R. Jacob. *CMOS*. Hoboken, NJ, USA: John Wiley & Sons, 2011.

[5] Beaucour, J., T. Carriere, A. Gach, and D. Laxague. "Total Dose Effects on Negative Voltage Regulator." *31. Annual International Nuclear and Space Radiation Effects Conference* 41.6 (1994): 2420-2426.

[6] Wei, A., S. L. Kosier, R. D. Schrimpf, D. M. Fleetwood, and W. E. Combs. "Dose-rate Effects on Radiation-induced Bipolar Junction Transistor Gain Degradation." *Applied Physics Letters*65.15 (1994): 1918-920. Web

[7] McClure, S., and R.L. Pease. "Dependence of Total Dose Response of Bipolar Linear Microcircuits on Applied Dose Rate." *IEEE Transactions on Nuclear Science* 41.6Pt1 (1994): IEEE Transactions on Nuclear Science, 1994, Vol.41(6Pt1).

[8] Barnaby, Tausch, Turfler, Cole, Baker, and Pease. "Analysis of Bipolar Linear Circuit Response Mechanisms for High and Low Dose Rate Total Dose Irradiations." *Nuclear Science, IEEE Transactions on* 43.6 (1996): 3040-048.

[9] Mcclure, S.S., J.L. Gorelick, R. Pease, and A.H. Johnston. "Dose Rate and Bias Dependency of Total Dose Sensitivity of Low Dropout Voltage Regulators." *Radiation Effects Data Workshop, 2000* (2000): 100-05.

[10] Adell, P.C., R.D. Schrimpf, W.T. Holman, J.L. Todd, S. Caveriviere, R.R. Cizmarik, and K.F. Galloway. "Total Dose Effects in a Linear Voltage Regulator." *Nuclear Science, IEEE Transactions on* 51.6 (2004): 3816-821.

[11] Chavez, R.M., B.G. Rax, L.Z. Scheick, and A.H. Johnston. "Total Ionizing Dose Effects in Bipolar and BiCMOS Devices." *Radiation Effects Data Workshop, 2005. IEEE* (2005): 144-48.

[12] Miyahira, T.F., B.G. Rax, and A.H. Johnston. "Total Dose Degradation of Low-dropout Voltage Regulators." *Radiation Effects Data Workshop, 2005. IEEE* (2005): 127-31.

[13] Johnston, A.H., and B.G. Rax. "Testing and Qualifying Linear Integrated Circuits for Radiation Degradation in Space." *Nuclear Science, IEEE Transactions on* 53.4 (2006): 1779-786.

[14] Pease, R.L., G.W. Dunham, and J.E. Seiler. "Total Dose and Dose Rate Response of Low Dropout Voltage Regulators." *Radiation Effects Data Workshop, 2006 IEEE* (2006): 85-93.

[15] Ramachandran, V. (2013). Analysis of total dose effects in a low-dropout voltage regulator. Available from ProQuest Dissertations & Theses Global.

[16] Kelly, A.T., P.C. Adell, A.F. Witulski, W.T. Holman, R.D. Schrimpf, and V. Pouget. "Total Dose and Single Event Transients in Linear Voltage Regulators." *Nuclear Science, IEEE Transactions on* 54.4 (2007): 1327-334.

[17] Chen, Dakai, James D. Forney, Ronald L. Pease, Anthony M. Phan, Martin A. Carts, Stephen R. Cox, Kirby Kruckmeyer, Sam Burns, Rafi Albarian, Bruce Holcombe, Bradley Little, James Salzman, Geraldine Chaumont, Herve Duperray, Al Ouellet, and Kenneth Label. "The Effects of ELDRS at Ultra-Low Dose Rates." Radiation Effects Data Workshop (REDW), 2010 IEEE (2010): 6.

[18] Privat, A., H. J. Barnaby, P. C. Adell, B. S. Tolleson, Y. Wang, X. Han, P. Davis, B. R. Rax, and T. E. Buchheit. "Multiscale Modeling of Total Ionizing Dose Effects in Commercial-off-the-Shelf Parts in Bipolar Technologies." IEEE Transactions on Nuclear Science66.1 (2019): 190-98.

[19] Titus, J.L., D. Emily, J.F. Krieg, T. Turflinger, R.L. Pease, and A. Campbell. "Enhanced Low Dose Rate Sensitivity (ELDRS) of Linear Circuits in a Space Environment." *IEEE Transactions on Nuclear Science* 46.6Pt1 (1999): 1608-1615.

[20] Wu, A., R.D. Schrimpf, H.J. Barnaby, D.M. Fleetwood, R.L. Pease, and S.L. Kosier. "Radiation-induced Gain Degradation in Lateral PNP BJTs with Lightly and Heavily Doped Emitters." *Nuclear Science, IEEE Transactions on* 44.6 (1997): 1914-921.

[21] Pease, R.L. "Evaluation of Proposed Hardness Assurance Method for Bipolar Linear Circuits with Enhanced Low Dose Rate Sensitivity (ELDRS)." *IEEE Transactions on Nuclear Science*45.6Pt1 (1998): 2665-672.

[22] Pease, R.L., D.G. Platteter, G.W. Dunham, J.E. Seiler, H.J. Barnaby, R.D. Schrimpf, M.R. Shaneyfelt, M.C. Maher, and R.N. Nowlin. "Characterization of Enhanced Low

Dose Rate Sensitivity (ELDRS) Effects Using Gated Lateral PNP Transistor Structures." *Nuclear Science, IEEE Transactions on* 51.6 (2004): 3773-780.

[23] Fleetwood, D.M., R.A. Jr. Reber, and P.S. Winokur. "Physical Mechanisms Contributing to Enhanced Bipolar Gain Degradation at Low Dose Rates." *31. Annual International Nuclear and Space Radiation Effects Conference* 41.6 (1994): 1871-1883.

[24] Fleetwood, D.M., L.C. Riewe, and J.R. Schwank. "Radiation Effects at Low Electric Fields in Thermal, SIMOX, and Bipolar-based Oxides." *IEEE Transactions on Nuclear Science* 43.6 (1996): 2537-546.

[25] Witczak, S.C., R.C. Lacoe, D.C. Mayer, D.M. Fleetwood, R.D. Schrimpf, and K.F. Galloway. "Space Charge Limited Degradation of Bipolar Oxides at Low Electric Fields." *Nuclear Science, IEEE Transactions on* 45.6 (1998): 2339-351.

[26] Rashkeev, Cirba, Fleetwood, Schrimpf, Witczak, Michez, Pantelides, and Rashkeev, S. "Physical Model for Enhanced Interface-trap Formation at Low Dose Rates." IEEE Transactions on Nuclear Science (0018-9499) 49.6 (2002): 2650-655.

[27] Belyakov, V.V., V.S. Pershenkov, A.V. Shalnov, and I.N. Shvetzov-Shilovsky. "Use of MOS Structures for the Investigation of Low-dose-rate Effects in Bipolar Transistors." *IEEE Transactions on Nuclear Science* 42.6Pt1 (1995): 1660-666.

[28] Boch, J., F. Saigne, R.D. Schrimpf, J.-R. Vaille, L. Dusseau, and E. Lorfevre. "Physical Model for the Low-Dose-Rate Effect in Bipolar Devices." *Nuclear Science, IEEE Transactions on* 53.6 (2006): 3655-660.

[29] Johnston, A.H., B.G. Rax, and C.I. Lee. "Enhanced Damage in Linear Bipolar Integrated Circuits at Low Dose Rate." *IEEE Transactions on Nuclear Science* 42.6Pt1 (1995): 1650-659.

[30] Shaneyfelt, M.R., R.L. Pease, J.R. Schwank, M.C. Maher, G.L. Hash, D.M. Fleetwood, P.E. Dodd, C.A. Reber, S.C. Witczak, L.C. Riewe, H.P. Hjalmarson, J.C. Banks, B.L. Doyle, and J.A. Knapp. "Impact of Passivation Layers on Enhanced Low-dose-rate Sensitivity and Pre-irradiation Elevated-temperature Stress Effects in Bipolar Linear ICs." *Nuclear Science, IEEE Transactions on* 49.6 (2002): 3171-179.

[31] Wei, A. "Excess Collector Current Due to an Oxide-trapped-charge-induced Emitter in Irradiated NPN BJT`s." *IEEE Transactions on Electron Devices* 42.5 (1995): 923-27.

[32] Kosier, S.L. "Physically Based Comparison of Hot-carrier-induced and Ionizing-radiation-induced Degradation in BJT`s." *IEEE Transactions on Electron Devices* 42.3 (1995): 436-44.

[33] Kosier, S.L., R.D. Shrimpf, R.N. Nowlin, D.M. Fleetwood, M. Delaus, R.L. Pease, W.E. Combs, A. Wei, and F. Chai. "Charge Separation for Bipolar Transistors." *Nuclear Science, IEEE Transactions on* 40.6 (1993): 1276-285.

[34] Schmidt, D.M., A. Wu, and R.D. Schrimpf. "Modeling Ionizing Radiation Induced Gain Degradation of the Lateral PNP Bipolar Junction Transistor." *IEEE Transactions on Nuclear Science*43.6Pt1 (1996): 3032-039.

[35] Hughart, D. R., R. D. Schrimpf, D. M. Fleetwood, N. L. Rowsey, M. E. Law, B. R. Tuttle, and S. T. Pantelides. "The Effects of Proton-Defect Interactions on Radiation-Induced Interface-Trap Formation and Annealing." *Nuclear Science, IEEE Transactions on*59.6 (2012): 3087-092.

[36] Hjalmarson, H.P., R.L. Pease, and R.A.B. Devine. "Calculations of Radiation Dose-Rate Sensitivity of Bipolar Transistors." *Nuclear Science, IEEE Transactions on* 55.6 (2008): 3009-015.

[37] Esqueda, I. S., H. J. Barnaby, P. C. Adell, B. G. Rax, H. P. Hjalmarson, M. L. Mclain, and R. L. Pease. "Modeling Low Dose Rate Effects in Shallow Trench Isolation Oxides." *Nuclear Science, IEEE Transactions on* 58.6 (2011): 2945-952.

[38] Tolleson, Adell, Rax, Barnaby, Privat, Han, Mahmud, and Livingston. "Improved Model for Excess Base Current in Irradiated Lateral P-n-p Bipolar Junction Transistors." *Nuclear Science, IEEE Transactions on* 65.8 (2018): 1488-495.

[39] Dodd, Paul Emerson, Leonard Charles Riewe, Ronald L. Pease, Marty Ray Shaneyfelt, Sunny Gupta, Michael C. Maher, and James Ralph Schwank. "Passivation Layers for Reduced Total Dose Effects and ELDRS in Linear Bipolar Devices." *Proposed for Publication in IEEE Transactions on Nuclear Science.* 50.6 (2003): 1784,1785,1786,1787,1788,1789,1790.

[40] Pease, Platteter, Dunham, Seiler, Adell, Barnaby, and Jie Chen. "The Effects of Hydrogen in Hermetically Sealed Packages on the Total Dose and Dose Rate Response of Bipolar Linear Circuits." *Nuclear Science, IEEE Transactions on* 54.6 (2007): 2168-173.

[41] Pease, Adell, Rax, Xiao Jie Chen, Barnaby, Holbert, and Hjalmarson. "The Effects of Hydrogen on the Enhanced Low Dose Rate Sensitivity (ELDRS) of Bipolar Linear Circuits." *Nuclear Science, IEEE Transactions on* 55.6 (2008): 3169-173.

[42] Adell, P.C., R.L. Pease, H.J. Barnaby, B. Rax, X.J. Chen, and S.S. Mcclure. "Irradiation with Molecular Hydrogen as an Accelerated Total Dose Hardness Assurance Test Method for Bipolar Linear Circuits." *Nuclear Science, IEEE Transactions on* 56.6 (2009): 3326-333.

[43] Adell, Philippe. C., Bernard Rax, Ivan S. Esqueda, and Hugh. J. Barnaby. "Hydrogen Limits for Total Dose and Dose Rate Response in Linear Bipolar Circuits." *IEEE Transactions on Nuclear Science* 62.6 (2015): 2476-481.

[44] Rax, B.G., C.I. Lee, and A.H. Johnston. "Degradation of Precision Reference Devices in Space Environments." *IEEE Transactions on Nuclear Science* 44.6Pt1 (1997): 1939-944.

[45] Auer, Mario, and Varvara Bezhenova. "A Radiation-hard Curvature Compensated Bandgap Voltage Reference." *Elektrotechnik Und Informationstechnik* 135.1 (2018): 3-9.

[46] Ramachandran, V., B. Narasimham, D.M. Fleetwood, R.D. Schrimpf, W.T. Holman, A.F. Witulski, R.L. Pease, G.W. Dunham, J.E. Seiler, and D.G. Platteter. "Modeling Total-Dose Effects for a Low-Dropout Voltage Regulator." *Nuclear Science, IEEE Transactions on* 53.6 (2006): 3223-231.

[47] Pease, R.L, R.D Schrimpf, and D.M Fleetwood. "ELDRS in Bipolar Linear Circuits: A Review." *IEEE Transactions on Nuclear Science* 56.4 (2009): 1894-908.

[48] Srour, J.R, and J.M Mcgarrity. "Radiation Effects on Microelectronics in Space." *Proceedings of the IEEE*76.11 (1988): 1443-469.

[49] Braäunig, D., and F. Wulf. "Atomic Displacement and Total Ionizing Dose Damage in Semiconductors." *Radiation Physics and Chemistry* 43.1-2 (1994): 105-27.

[50] Barnaby, H.J. "Total-Ionizing-Dose Effects in Modern CMOS Technologies." *IEEE Transactions on Nuclear Science* 53.6 (2006): 3103-121.

[51] Campbell, Phillip M, and Carolyn W Bogden. *Analytical Models for Total Dose Ionization Effects in MOS Devices.* Sandia National Laboratories, *Analytical Models for Total Dose Ionization Effects in MOS Devices.*

[52] Borghello, G., Faccio, Lerario, Michelis, Kulis, Fleetwood, Schrimpf, Gerardin, Paccagnella, and Bonaldo. "Dose-Rate Sensitivity of 65-nm MOSFETs Exposed to Ultrahigh Doses." *IEEE Transactions on Nuclear Science* 65.8 (2018): 1482-487.

[53] Witczak, S., Lacoe, Osborn, Hutson, and Moss. "Dose-rate Sensitivity of Modern NMOSFETs." *IEEE Transactions on Nuclear Science* 52.6 (2005): 2602-608.

[54] Campola, Michael, Barnaby, Hugh J., Holbert, Keith, and Vasileska, Dragica. *Separating Radiation and Thermal Effects on Lateral PNP Bipolar Junction Transistors Operating in the Space Environment* (2011): ProQuest Dissertations and Theses.